

[Click here to view linked References](#)

This is the Pre-Published Version.

Bulletin of Earthquake Engineering manuscript No.
(will be inserted by the editor)

This version of the article has been accepted for publication, after peer review (when applicable) and is subject to Springer Nature's AM terms of use (<https://www.springernature.com/gp/open-research/policies/accepted-manuscript-terms>), but is not the Version of Record and does not reflect post-acceptance improvements, or any corrections. The Version of Record is available online at: <https://doi.org/10.1007/s10518-020-00865-5>.

Seismic Loss and Resilience Assessment of **Single-Column** Rocking Bridges

Anastasios I. Giouvanidis ·
You Dong

Received: date / Accepted: date

Abstract This study focuses on structural systems, which are particularly attractive for bridge design. Specifically, it investigates the seismic performance of single-column bridges, which are either conventionally designed, with the column monolithically connected with the ground (i.e. fixed-base), or designed with the column-footing system able to uplift and exhibit planar rocking motion during an earthquake. Although various researchers have studied the examined structures in terms of their seismic fragility, their seismic losses, post-earthquake functionality and resilience have received less attention. This paper redirects our attention to the main benefits of rocking design over the conventional (fixed-base) design in the aftermath of severe seismic hazard scenarios. The analysis reveals the considerably mitigated (short-term and long-term) seismic losses of the rocking structure compared to the pertinent losses of the fixed-base structure. In addition, the results show the remarkable functionality and resilience of the rocking structure after all the examined seismic hazard scenarios. **Importantly, this work unveils that the post-earthquake financial benefits of the rocking structure can be further increased when the structure is carefully designed. In particular, even a small modification of its slenderness can lead to a substantial enhancement of its post-earthquake performance.** The above findings illustrate the potential of the **rocking structural system** as an alternative seismic design paradigm for bridges and serve as the basis for a more rational and holistic seismic assessment framework of single-column rocking bridges.

Keywords rocking · analytical dynamics · fragility · seismic loss · post-earthquake functionality · resilience

1 Introduction

Conventional bridge seismic design provides the necessary strength and ductility to the structure to withstand seismic forces and avoid collapse. Such a design concept, though, accepts the “*prize*” of sustainable seismic damage and subsequently residual displacements

Anastasios I. Giouvanidis · You Dong ✉
Department of Civil and Environmental Engineering, The Hong Kong Polytechnic University, Hung Hom, Kowloon, Hong Kong
E-mail: agiouv@polyu.edu.hk · you.dong@polyu.edu.hk

after severe earthquakes. Seismic damage is an important measure of post-earthquake functionality that often determines whether or not a bridge remains operational following a seismic event [55,58]. Rocking design, on the other hand, as an alternative seismic isolation technique, aims to relieve the structure from seismic damage by allowing structural components to uplift and pivot during an earthquake [61]. The seminal work of Housner [50] first revealed the benefits of rocking design over the conventional (fixed-base) design after the Chilean earthquake in 1960. That study triggered the analytical [34,33,29,35,3,92,91,27,12,81], numerical [93,94,32] and experimental [88,4,21,10] investigation of the benefits of rocking isolation on various structural applications, e.g. classical monuments [30,80], critical contents [56,31], buildings [54,11,77] and bridges [62,36,46,67].

The mechanical configuration of Fig. 1(a), where the column is monolithically connected with the ground (i.e. fixed-base), is particularly attractive for bridge design. One way to implement rocking isolation is by designing the column to be monolithically connected with the footing (or base), while the column-base system can detach from the (assumed rigid) ground when subjected to a ground motion. Hence, the rocking **structural system** of e.g. Fig. 1(b) is gaining momentum as an alternative bridge design paradigm, since it combines the benefits of rocking isolation with the merits of the Accelerated Bridge Construction (ABC) method [64,86,85]. To illustrate its superior behavior, various studies investigated its seismic performance in comparison to its fixed-base counterpart through either advanced numerical (finite element) models [74,7,5] or experimental tests [66,51,87,75,98,82]. Those studies highlighted, among others: (i) the mitigated seismic forces that are transmitted to the column of the rocking structure; and (ii) the negligible seismic damage and small residual displacements of the rocking structure compared to the substantial inelastic deformations and damage of the fixed-base structure (e.g. 0.4% versus 6.8% residual drift ratio, respectively, while both structures sustain almost the same peak drift ratio).

On the other hand, the analytical studies that compare the structures of Fig. 1 still remain scarce. Modelling the structural systems of Fig. 1(a) and Figs 1(b), 1(c) as a single and a two degree-of-freedom oscillator, respectively, Chopra and Yim [23] and Psycharis [79] were (probably) the first that made such a comparison assuming small rocking rotations for the uplifted structure. **Those studies showed that, based on the structural characteristics, the uplifted structure can sustain smaller deformations (i.e. drifts) than the fixed-base structure**, verifying preliminary results from Meek [68]. More recently, Oliveto et al. [72] verified the conclusions of [23,79] assuming large rotations (i.e. considering overturning of the rocking structure). In this context, Vassiliou et al. [95] highlighted that more flexible rocking structures exhibit smaller deformations than fixed-base structures (with the same stiffness). On the contrary, stiffer rocking structures tend to oscillate strongly after each impact, thus, larger deformations occur. Xie et al. [99] compared the structural systems of Fig. 1 in terms of their seismic fragility and unveiled an optimal range of slenderness (i.e. $\pi/15 < \alpha < \pi/10$) that significantly reduces both the overturning tendency and the damage probability of the rocking structure compared to its fixed-base counterpart.

This study is motivated by the lack of analytical studies that thoroughly evaluate the performance of the structural systems of Fig. 1 after severe seismic events. In particular, most analytical studies compare the examined structures solely in terms of their seismic fragility. However, due to their inherently different structural characteristics, a comparison only via fragility analysis would be unfair and incomplete. Hence, this work extends recent studies [99] by conducting a comparative analysis of the structural systems of Fig. 1 in terms of their: (i) (short-term) seismic (repair) losses adopting the performance-based earthquake engineering framework; (ii) long-term seismic losses; (iii) post-earthquake functionality; and (iv) resilience adopting a more holistic resilience-based earthquake engineering framework.

In this context, the analysis herein provides an insight on the seismic performance of rocking bridges by investigating the influence of design parameters (i.e. slenderness) on the seismic losses, post-earthquake functionality and resilience, and it examines whether or not rocking design can be an economically feasible solution for future bridge engineering applications. Therefore, this research study: (i) redirects our attention to the main benefits of rocking design over the conventional (fixed-base) design (e.g. seismic losses, post-earthquake functionality, resilience); and (ii) paves the way for a more holistic seismic assessment framework of single-column rocking bridges.

2 Analytical Modelling of **Single-Column** Rocking Bridges

2.1 Equations of Motion

Fig. 1 illustrates the examined single-column **structural systems**. Fig. 1(a) shows the conventional (fixed-base) design, while Figs 1(b), 1(c) illustrate the rocking column-base system that is designed for bridges. Assuming rigid ground conditions and no sliding at the rocking interface allow the structures of Figs 1(b), 1(c) to uplift and pivot during an earthquake exhibiting planar rocking motion. This is a simplification of the present study. However, the design method of the rocking structures justifies these assumptions. Specifically, the piles used to facilitate the monolithic connection of the fixed-base structure with the ground (Fig. 1(a)) are also installed at the ground where the rocking structures lay (Figs 1(b), 1(c)). In this context, the piles can serve both as shear keys to prevent sliding at the rocking interface [7] and as ground reinforcement to support the assumption of rigid ground conditions [76].

When the rocking structures of Figs 1(b), 1(c) remain in full contact with the ground, from a dynamics perspective, they behave as a single degree-of-freedom system (i.e. similar to the fixed-base **structure** of Fig. 1(a)). Thus, their motion is captured by the deformation of the column u . After rocking commences, the motion of the rocking **structures** is captured by both the deformation of the column u and the rocking rotation ϕ of the base (see e.g. Fig. 1(b)). Hence, the structural systems of Fig. 1 can be modelled as either a single degree-of-freedom oscillator fixed on the ground (Fig. 1(a)) or a two degree-of-freedom oscillator able to uplift and rock (Figs 1(b), 1(c)) [1,2,45,95].

Consider the rocking oscillator of e.g. Fig. 1(b) with a concentrated mass m at height h . The column has a total mass of m_c and elastic stiffness of EI uniformly distributed along its length. The rigid base has mass m_b and width $2b$, while its height is considered negligible compared to its width. For simplicity, assume the lumped mass m creates no moment of inertia [21,100,99] (see e.g. [41] for a more detailed structural modelling of a single-column rocking bridge). The rigid base creates moment of inertia with respect to its center of mass equal to $I_{m_b} = (1/3) m_b b^2$. The shape function that describes the deformation of the column is [22,95,45]:

$$\psi(\xi) = \frac{3\xi^2}{2h^2} - \frac{\xi^3}{2h^3} \quad (1)$$

where ξ is the distance measured from the base of the column (see e.g. Fig. 1(b)). The deformation of any arbitrary point along the column is defined as $u_\xi(\xi, t) = u(t) \cdot \psi(\xi)$. Recall that, before rocking initiates, the oscillator behaves as a single degree-of-freedom

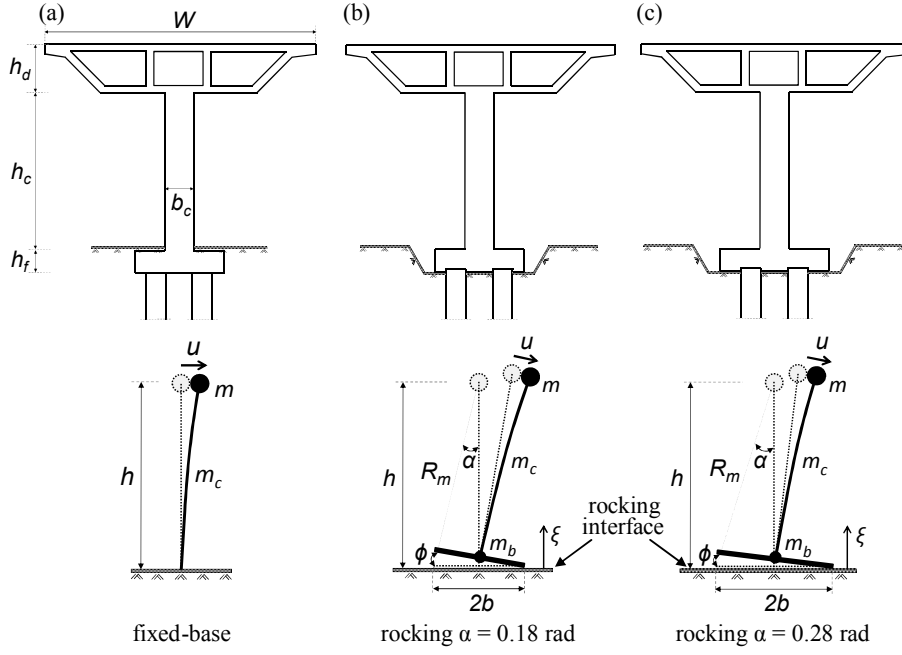


Fig. 1 Single-column bridge: (a) designed conventionally with the column monolithically connected with the ground (i.e. fixed-base); and (b), (c) designed to uplift and pivot during an earthquake with the column-base system isolated from the ground (i.e. rocking with slenderness $\alpha = 0.18$ rad, $\alpha = 0.28$ rad, respectively)

system with generalized mass and stiffness respectively [95,45]:

$$\begin{aligned}\tilde{m} &= m + \int_0^h \frac{m_c}{h} (\psi(\xi))^2 d\xi = m + \frac{33}{140} m_c \\ \tilde{k} &= \int_0^h EI (\psi''(\xi))^2 d\xi = \frac{3EI}{h^3}\end{aligned}\quad (2)$$

At an arbitrary time-instant after the initiation of rocking, the position of the lumped mass (X_m, Y_m) , any point along the column (X_{m_c}, Y_{m_c}) and the midpoint of the rigid base (X_{m_b}, Y_{m_b}) can be expressed as:

$$\begin{cases} X_m = u_g(t) - \text{sgn}(\phi) b \cos \phi + h \sin \phi + u \cos \phi \\ Y_m = \text{sgn}(\phi) b \sin \phi + h \cos \phi - u \sin \phi \\ X_{m_c} = u_g(t) - \text{sgn}(\phi) b \cos \phi + \xi \sin \phi + u \psi \cos \phi \\ Y_{m_c} = \text{sgn}(\phi) b \sin \phi + \xi \cos \phi - u \psi \sin \phi \\ X_{m_b} = u_g(t) - \text{sgn}(\phi) b \cos \phi \\ Y_{m_b} = \text{sgn}(\phi) b \sin \phi \end{cases}\quad (3)$$

where $u_g(t)$ denotes the ground displacement measured from a reference point on the ground and $\text{sgn}(\phi)$ is the signum function of the rocking rotation ϕ .

The equations of motion of the rocking oscillator of Figs 1(b), 1(c) can be derived using the general form of the Lagrange's equation:

$$\frac{d}{dt} \left(\frac{\partial L}{\partial \dot{u}} \right) - \frac{\partial L}{\partial u} = Q \quad (4)$$

$$\frac{d}{dt} \left(\frac{\partial L}{\partial \dot{\phi}} \right) - \frac{\partial L}{\partial \phi} = 0 \quad (5)$$

where $L = T - V$, with T the kinetic energy, V the potential energy and Q the generalized force. In particular, the kinetic energy of the rocking structure is expressed as:

$$\begin{aligned} T = \frac{1}{2}m & \left(h^2 \dot{\phi}^2 + 2h\dot{\phi}\dot{u} + \dot{u}^2 + u^2 \dot{\phi}^2 + b^2 \dot{\phi}^2 - \text{sgn}(\phi) 2bu\dot{\phi}^2 \right. \\ & \left. + \dot{u}_g^2 + \text{sgn}(\phi) 2\dot{u}_g b \sin \phi \dot{\phi} + 2\dot{u}_g h \cos \phi \dot{\phi} + 2\dot{u}_g \dot{u} \cos \phi - 2\dot{u}_g u \sin \phi \dot{\phi} \right) \\ & + \frac{1}{2}I_{m_b} \dot{\phi}^2 + \frac{1}{2}m_b \left(\dot{u}_g^2 + \text{sgn}(\phi) 2\dot{u}_g b \sin \phi \dot{\phi} + b^2 \dot{\phi}^2 \right) \\ & + \frac{1}{2}m_c \left(\frac{h^2}{3} \dot{\phi}^2 + \frac{33}{140} \dot{u}^2 + \frac{33}{140} u^2 \dot{\phi}^2 + \frac{11}{20} h\dot{u}\dot{\phi} + b^2 \dot{\phi}^2 - \text{sgn}(\phi) \frac{3}{4} bu\dot{\phi}^2 \right. \\ & \left. + \dot{u}_g^2 + \text{sgn}(\phi) 2\dot{u}_g b \sin \phi \dot{\phi} + h\dot{u}_g \cos \phi \dot{\phi} + \frac{3}{4} \dot{u}_g \dot{u} \cos \phi - \frac{3}{4} \dot{u}_g u \sin \phi \dot{\phi} \right) \end{aligned} \quad (6)$$

where \dot{u} , $\dot{\phi}$ and \dot{u}_g denote the flexural, angular and ground velocity, respectively. The potential energy due to the gravitational forces and the strain energy of the rocking structure becomes:

$$\begin{aligned} V = \frac{3EI}{2h^3} u^2 + mg & \left(\text{sgn}(\phi) b \sin \phi + h \cos \phi - u \sin \phi \right) \\ & + \text{sgn}(\phi) m_b g b \sin \phi + m_c g \left(\text{sgn}(\phi) b \sin \phi + \frac{h}{2} \cos \phi - \frac{3}{8} u \sin \phi \right) \end{aligned} \quad (7)$$

Further, the work done by the non-conservative forces gives the generalized force Q :

$$\delta W_{nc} = Q\delta u = -C\dot{u}\delta u \quad (8)$$

where C is the damping coefficient responsible for the energy dissipation while the structure vibrates. After substituting Eqs (6), (7), (8) into Eqs (4), (5), the equations that describe the motion of the rocking oscillator of Figs 1(b), 1(c) become:

$$\begin{aligned} \left(m + \frac{33}{140} m_c \right) \ddot{u} + \left(m + \frac{11}{40} m_c \right) h \ddot{\phi} = \\ -C\dot{u} - \frac{3EI}{h^3} u + \left[\left(m + \frac{33}{140} m_c \right) u - \text{sgn}(\phi) \left(m + \frac{3}{8} m_c \right) b \right] \dot{\phi}^2 \\ - \dot{u}_g \left(m + \frac{3}{8} m_c \right) \cos \phi + g \left(m + \frac{3}{8} m_c \right) \sin \phi \end{aligned} \quad (9)$$

$$\begin{aligned} \left(m + \frac{11}{40} m_c \right) h \ddot{u} + \left[\left(I_{m_b} + m_b b^2 \right) + m \left(h^2 + b^2 \right) + mu^2 - \text{sgn}(\phi) 2mbu \right] \ddot{\phi} = \\ + m_c \left(\frac{1}{3} h^2 + b^2 \right) + \frac{33}{140} m_c u^2 - \text{sgn}(\phi) \frac{3}{4} m_c bu \\ - \left(2m + \frac{33}{70} m_c \right) u \dot{\phi} + \text{sgn}(\phi) \left(2m + \frac{3}{4} m_c \right) b \dot{u} \dot{\phi} \\ + \ddot{u}_g \left[\begin{array}{l} -\text{sgn}(\phi) \left(m + m_b + m_c \right) b \sin \phi \\ - \left(m + \frac{1}{2} m_c \right) h \cos \phi + \left(m + \frac{3}{8} m_c \right) u \sin \phi \end{array} \right] \\ + g \left[\begin{array}{l} -\text{sgn}(\phi) \left(m + m_b + m_c \right) b \cos \phi \\ + \left(m + \frac{1}{2} m_c \right) h \sin \phi + \left(m + \frac{3}{8} m_c \right) u \cos \phi \end{array} \right] \end{aligned} \quad (10)$$

in agreement with [95]. \ddot{u} and $\ddot{\phi}$ denote the flexural and angular acceleration, while \ddot{u}_g and g are the ground and gravitational acceleration, respectively.

Before rocking commences, the motion of both the fixed-base **structure** of Fig. 1(a) and the rocking **structures** of Figs 1(b), 1(c) can be captured solely by the flexural deformation of the column u . Hence, assuming $\phi = 0$, $\dot{\phi} = 0$ and $\ddot{\phi} = 0$, Eq. (9) yields the equation of motion of the fixed-base oscillator of Fig. 1(a) and the rocking oscillator of Figs 1(b), 1(c) when it is in full contact with the ground.

$$\left(m + \frac{33}{140} m_c \right) \ddot{u} = -C\dot{u} - \frac{3EI}{h^3} u - \ddot{u}_g \left(m + \frac{3}{8} m_c \right) \quad (11)$$

2.2 Rocking Initiation

Rocking initiates when the overturning moment M_{OT} due to the external forces exceeds the restoring moment M_R of the structural system. Eq. (10) represents the moment equilibrium of the rocking oscillator of e.g. Fig. 1(b) with respect to its pivot points including all the forces that act on the body (e.g. seismic, gravitational, elastic, etc.). Recall that the rate of change of the angular momentum about a point (e.g. the pivot point) is equal to the sum of the moments (i.e. $M = M_{OT} + M_R$) of forces acting on the body about that point. Therefore, Eq. (10) can be re-written as:

$$\underbrace{\left[(I_{m_b} + m_b b^2) + m (h^2 + b^2) + mu^2 - 2mbu \right]}_{M_{OT}} \ddot{\phi} = \underbrace{\left[+m_c \left(\frac{1}{3}h^2 + b^2 \right) + \frac{33}{140}m_c u^2 - \frac{3}{4}m_c bu \right]}_{M_R} - \left(m + \frac{11}{40}m_c \right) h \ddot{u} - \ddot{u}_g \left(m + \frac{1}{2}m_c \right) h - g \left[(m + m_b + m_c) b - \left(m + \frac{3}{8}m_c \right) u \right] \quad (12)$$

for clockwise (positive) rotations, and

$$\underbrace{\left[(I_{m_b} + m_b b^2) + m (h^2 + b^2) + mu^2 + 2mbu \right]}_{M_{OT}} \ddot{\phi} = \underbrace{\left[+m_c \left(\frac{1}{3}h^2 + b^2 \right) + \frac{33}{140}m_c u^2 + \frac{3}{4}m_c bu \right]}_{M_R} - \left(m + \frac{11}{40}m_c \right) h \ddot{u} - \ddot{u}_g \left(m + \frac{1}{2}m_c \right) h - g \left[-(m + m_b + m_c) b - \left(m + \frac{3}{8}m_c \right) u \right] \quad (13)$$

for counter-clockwise (negative) rotations assuming $\phi = 0$ and $\dot{\phi} = 0$. Uplift occurs when $M > 0$ for clockwise (positive) rotations and $M < 0$ for counter-clockwise (negative) rotations. Therefore, Eqs (12), (13) give:

$$\mp \left(m + \frac{11}{40}m_c \right) h \ddot{u} \mp \ddot{u}_g \left(m + \frac{1}{2}m_c \right) h - g \left[\frac{(m + m_b + m_c) b}{\mp \left(m + \frac{3}{8}m_c \right) u} \right] > 0 \quad (14)$$

where the upper sign denotes clockwise (positive) rotations and the lower sign counter-clockwise (negative) rotations. With the aid of Eq. (11), the uplift condition becomes:

$$\pm h \frac{m + \frac{11}{40}m_c}{m + \frac{33}{140}m_c} \left[C \dot{u} + \frac{3EI}{h^3} u \right] \mp \ddot{u}_g \left(m + \frac{1}{2}m_c \right) h - g \left[\frac{(m + m_b + m_c) b}{\mp \left(m + \frac{3}{8}m_c \right) u} \right] > 0 \quad (15)$$

in agreement with [95].

2.3 Impact Mechanism

During rocking, the smooth motion of the structure is interrupted by nonsmooth events (i.e. impacts) when $\phi = 0$, and energy is lost. The work of Housner [50] was one of the first to treat the impact phenomenon of a rigid rocking block. That study assumed impact as an instantaneous event. To capture the energy loss at impact, Housner [50] applied the conservation of angular momentum and introduced a coefficient of restitution that connects the pre-impact with the post-impact angular velocity.

After Housner's seminal work [50], various analytical methodologies have been proposed to capture the impact phenomenon of both rigid and flexurally deformable rocking

structures. Focusing on flexurally deformable rocking oscillators (e.g. Fig. 1(b)), Acikgoz and DeJong [1] assumed that the post-impact state is either immediate rocking or full contact with the ground, with the state of less total energy to govern. Vassiliou et al. [95] extended the model of Chopra and Yim [23] to large rocking rotations and assumed that the kinetic energy associated with the vertical components of the flexural velocity is lost at impact. Later, Acikgoz and DeJong [2] revisited the impact problem and simulated the impact behavior with impulsive Dirac-delta forces extending the model initially proposed in [78] for rigid bodies. Giouvanidis and Dimitrakopoulos [45] proposed a nonsmooth dynamics methodology to capture all physically feasible post-impact states (i.e. full contact, immediate rocking, bouncing and/or simultaneous detachment of all contact points). That study showed that the post-impact state of a rocking oscillator is response-dependent. However, recall that immediate rocking becomes feasible only when the rocking oscillator is either very slender (i.e. $h/b > 10$) or it sustains excessive flexural deformations (i.e. $|u_{max}|/b > 1$) [45], which is not the case herein (as shown in Section 3.2 and Figs 5(e), 6(e), respectively, later on). Further, **small-scale** experiments have shown no immediate rocking as a post-impact state for a rocking oscillator [88]. In this context, Zhang et al. [100] assumed that after impact the rocking oscillator remains in full contact with the ground. That impact model showed satisfactory results in terms of the energy lost at each impact when compared to previous analytical models [1, 95].

Thus, following [100], this work assumes that after each impact the rocking oscillator of Figs 1(b), 1(c) remains in full contact with the ground and uplifts when the condition of Eq. (15) is met. **Note that the impact behavior of a small-scale rocking oscillator might not necessarily be the same with the impact behavior of a large-scale rocking bridge column. This is a limitation of the present study. However, whether a different impact model might significantly affect the rocking response merits further investigation, which is beyond the scope of the present study.** Under these assumptions, due to the instantaneous duration of impact $u^+ = u^- = u$. Further, since impact occurs $\phi^+ = \phi^- = 0$, and since the oscillator remains in full contact with the ground after impact $\dot{\phi}^+ = 0$. Therefore, the sole post-impact unknown is the flexural velocity \dot{u}^+ . Conservation of angular momentum gives [95]:

$$\dot{u}^+ = \dot{u}^- + \frac{I_{m_b} - m_b b^2 + m_c \left(-b^2 + \frac{1}{3}h^2 + \frac{33}{140}u^2\right) + m \left(-b^2 + h^2 + u^2\right)}{\left(m + \frac{11}{40}m_c\right) h} \dot{\phi}^- \quad (16)$$

where \dot{u}^- and $\dot{\phi}^-$ denote the pre-impact flexural and angular velocity, respectively. Assuming $m_b = 0$ and $m_c = 0$, Eq. (16) verifies the pertinent equation in [100].

3 Performance-Based Earthquake Engineering Assessment of **Single-Column Rocking Bridges**

To evaluate the seismic performance of a structural system, the Pacific Earthquake Engineering Research (PEER) Center proposed the *performance-based earthquake engineering* (PBEE) framework [40, 69]. The PBEE analysis allows for a quantitative assessment of the seismic performance of a structural system in terms of engineering parameters, such as the expected seismic losses accumulated in the aftermath of an earthquake. The PBEE framework encompasses four steps: (i) hazard analysis; (ii) structural analysis; (iii) damage analysis; and (iv) loss analysis. Fig. 2 illustrates the PBEE framework. Specifically, given a site location of the structure, the probabilistic seismic hazard analysis (PSHA) determines the

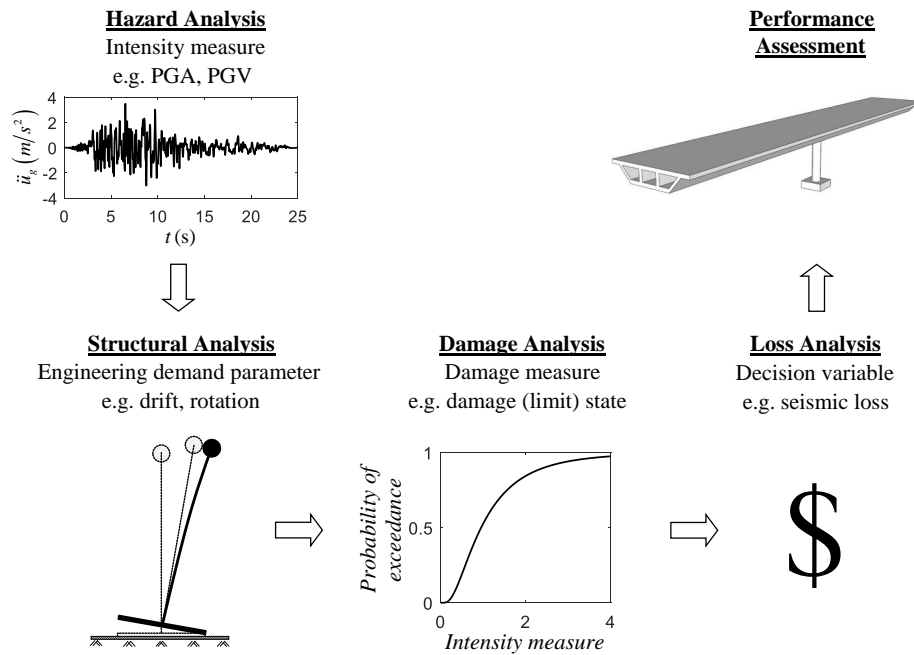


Fig. 2 Performance-based earthquake engineering framework

intensity measure(s) (IM(s)) extracted from the earthquake ground motions that are probable to occur in that area. Then, given the adopted IM(s), the structural analysis performs simulations to determine the engineering demand parameter(s) (EDP(s)) that is (are) regarded as measure(s) of the structural response. Given the adopted EDP(s), the damage analysis calculates the probability that the examined structural system will experience a certain level of damage quantified via damage limit states/measures. Finally, given the levels of damage that the structure sustains, the loss analysis connects the damage limit states/measures with decision variables, which are expressed in monetary values and can be easily assessed by the decision makers.

3.1 Hazard Analysis

To perform the PSHA, this section adopts the methodology proposed in [17, 14]. Assume that the examined **structural systems** of Fig. 1 are located in California laying on a strike-slip fault. The minimum and maximum moment magnitudes M_w are taken as 5.5 and 8, respectively, while the shear wave velocity averaged over the top 30 m $V_{s,30}$ is 480 m/s. The Joyner-Boore distance R_{JB} that characterizes the shortest distance between the site and the surface projection of the fault plane is taken as 5 km. The IM considered herein is the peak ground velocity (PGV) as it was shown to be the most critical for overturning various rocking configurations [37, 47]. The PSHA provides a sample of 1,000,000 PGV values of ground excitations that are probable to appear in the area of focus. Fig. 3(a) illustrates the distribution of the earthquake intensities expressed via the PGV sample with mean value 0.28 m/s and standard deviation 0.26 m/s.

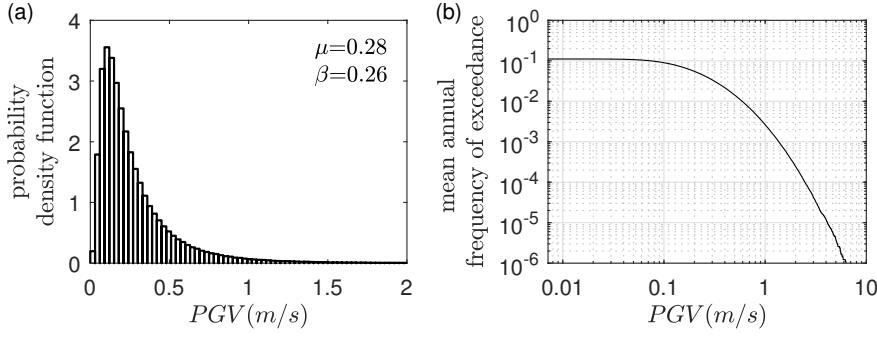


Fig. 3 (a) Probability density function of the generated PGV sample and (b) hazard curve (in logarithmic scale) for the area of focus after conducting the probabilistic seismic hazard analysis

To connect the earthquake events that are likely to appear in the examined area (i.e. California) with their annual frequency of exceedance, the Gutenberg-Richter recurrence law is adopted [48]:

$$\log_{10} \lambda_M = A - B \cdot M \quad (17)$$

where λ_M is the frequency of the earthquakes with magnitudes greater than M , while A and B are constants equal to 3.94 and 0.89, respectively [89]. Fig. 3(b) plots the hazard curve (in logarithmic scale) that provides the mean annual frequency of exceedance λ_M of every earthquake that is likely to occur in the area of focus characterized by the adopted PGV sample of Fig. 3(a).

3.2 Structural Analysis

This section investigates the seismic response of the single-column **structural systems** of Fig. 1. Each **structure** is considered to be part of a two-span box-girder bridge of total length $L = 60$ m and width $W = 10$ m. **Assume that the total mass of the column m_c is 25% of the total lumped mass m for all structural systems of Fig. 1, while the total mass of the base m_b is 15% of the total lumped mass m for the structure of Fig. 1(b) and 17% of the total lumped mass m for the structure of Fig. 1(c), respectively.** The lumped mass m is located at height $h = 8$ m. **The rocking structure of Fig. 1(b) has base-width $2b = 3$ m [100,99] and slenderness $\alpha = 0.18 \text{ rad} = \pi/17$ (i.e. $\alpha < \pi/15$ as reported in [99]), while the rocking structure of Fig. 1(c) has base-width $2b = 4.6$ m and slenderness $\alpha = 0.28 \text{ rad} = \pi/11$ (i.e. $\pi/15 < \alpha < \pi/10$ as reported in [99]).** For consistency, the examined **structural systems** have identical natural frequency $\omega_n = 8p$, where $p = \sqrt{g/R_m}$ is the frequency parameter of the rocking oscillator with R_m being the diagonal distance of the lumped mass from the pivot point (see e.g. Fig. 1(b)). The damping ratio ζ is taken equal to 5% for the fixed-base oscillator of Fig. 1(a). For the rocking oscillator of Figs 1(b), 1(c), after rocking commences, the damping ratio, in theory, is increased compared to the pertinent damping ratio when the rocking oscillator is in full contact with the ground [23, 79, 72, 1, 95]. Due to the lack of large-scale experiments that propose appropriate damping values for rocking bridge columns, this study follows [95, 45] and assumes a constant damping ratio of 5% during rocking and a reduced damping ratio value during full contact (see e.g. [95] for further details).

To connect the IM created during the PSHA (Section 3.1), appropriate EDPs for both structural configurations need first to be defined. Based on Section 2, the two EDPs used in

this study are: (i) the absolute peak flexural deformation $|u_{max}|$ normalized with respect to the height h (Eq. (18)); and (ii) the absolute peak rocking rotation $|\phi_{max}|$ normalized with respect to the slenderness α (Eq. (19)).

$$EDP_1 = \frac{|u_{max}|}{h} \quad (18)$$

$$EDP_2 = \frac{|\phi_{max}|}{\alpha} \quad (19)$$

The two EDPs of Eqs (18), (19) describe completely the motion of the **structural systems** of Fig. 1. Specifically, when rocking motion is allowed, the structures of Figs 1(b), 1(c) might initiate rocking (i.e. rocking simulations $|\phi_{max}|/\alpha > 0$) or not (i.e. nonrocking simulations $|\phi_{max}|/\alpha = 0$). In case the structures do not commence rocking (i.e. nonrocking simulations), from a dynamics perspective, they behave as a single degree-of-freedom oscillator (i.e. as the fixed-base structure of Fig. 1(a)). Thus, their motion is completely captured by the flexural deformation $|u_{max}|/h$. On the other hand, when rocking commences, a percentage of the rocking cases end with overturning (i.e. rocking overturning simulations), where $|\phi_{max}|/\alpha$ attains, in theory, an arbitrarily large value. The remaining rocking cases terminate without overturning (i.e. safe rocking simulations) and they yield in-between (nonzero) values of $|\phi_{max}|/\alpha$.

Each of the structural systems of Fig. 1 is subjected to a series of strong ground motions adopted from the Pacific Earthquake Engineering Research (PEER) Center database (i.e. **Tables A1, A2, A3, A4** in [15]). The database covers a wide range of both pulse-type and nonpulse-type ground motions with magnitudes $6 \leq M_w \leq 8$ and distance from the fault $R_{rup} \leq 50$ km. The adopted ground motions consist of two horizontal components and one vertical. Both horizontal components are used separately, while the vertical component is ignored. **To induce higher levels of demand, a scale factor of 1, 1.25 and 1.5 is, respectively, assigned to the accelerograms of the adopted database [90].** To preserve the kinematic features of the ground motions, larger scale factors have not been used. Therefore, 960 response-history analyses are conducted for each of the examined structural systems of Fig. 1.

Figs 4, 5, 6 illustrate the seismic response of the fixed-base structure (Fig. 4) and the rocking structures with slenderness $\alpha = 0.18$ rad (Fig. 5) and $\alpha = 0.28$ rad (Fig. 6) with respect to the adopted ground motion intensity measure. As a first approach, comparison of Figs 4, 5(b) reveals that rocking motion considerably reduces the structural deformation

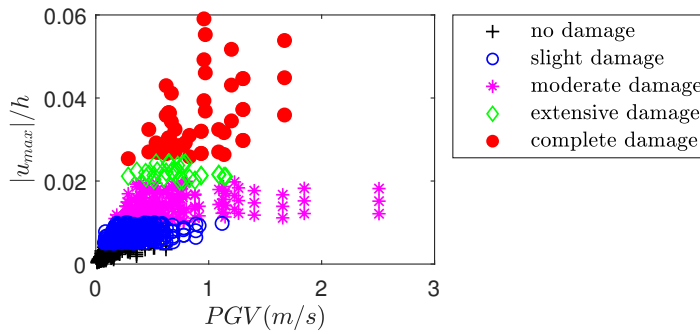


Fig. 4 Seismic response analysis of the conventionally designed (fixed-base) **structure** of Fig. 1(a)

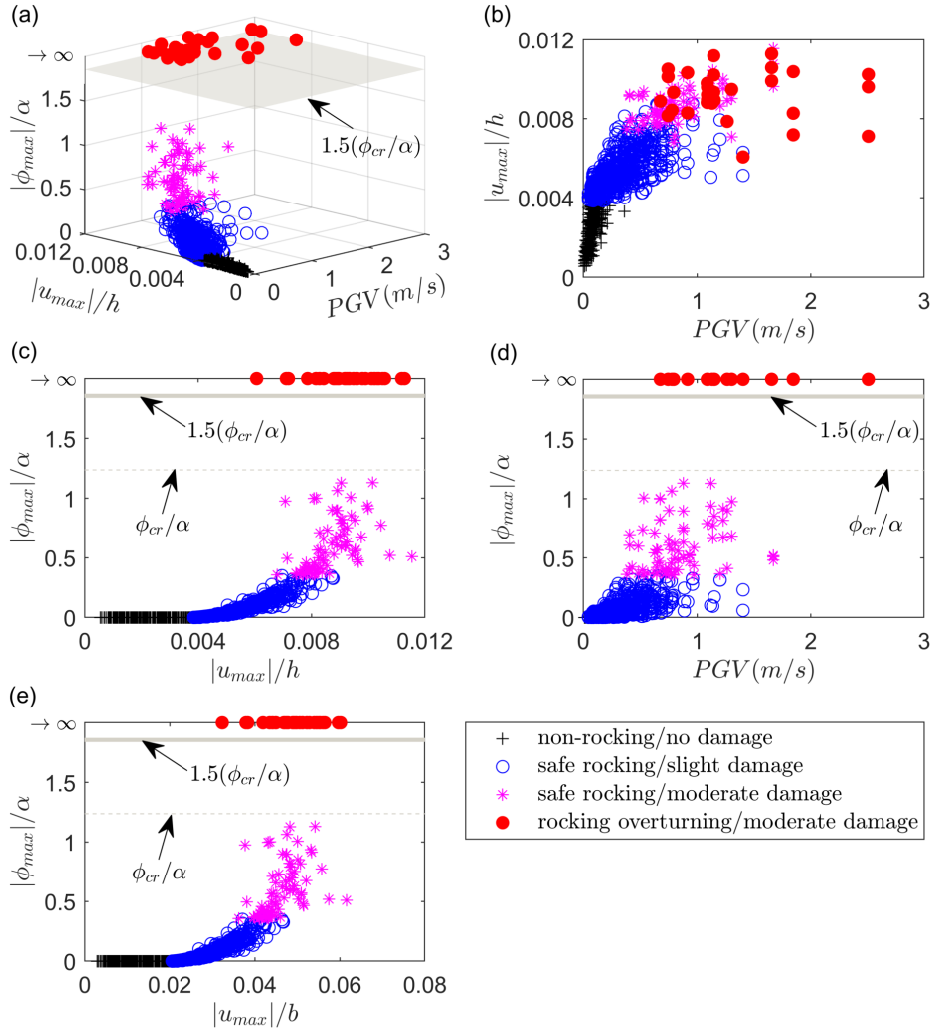


Fig. 5 Seismic response analysis of the rocking structure of Fig. 1(b) (i.e. $\alpha = 0.18$ rad)

$|u_{\max}|/h$ and therefore damage at the column. In addition, Figs 5, 6 unveil that increasing the slenderness of the structure mitigates the rocking response $|\phi_{\max}|/\alpha$. However, Figs 5(c), 6(c) show that increase of the slenderness leads also to slight increase of the structural deformation $|u_{\max}|/h$ and subsequently potentially higher levels of damage. Further, Figs 5(c), 6(c) show that after a certain limit of rotation (i.e. $|\phi_{\max}|/\alpha = 0.4-0.5$) no considerable increase on the structural deformation occurs. Finally, both Figs 5, 6 illustrate that when the rotation $|\phi_{\max}|/\alpha$ exceeds the critical rotation ϕ_{cr}/α [95], the structure becomes dynamically unstable and overturns. To be more conservative and capture cases beyond the present analysis, though, this study assumes that rocking angle $|\phi_{\max}|/\alpha$ larger than 1.5 times the critical rotation ϕ_{cr}/α leads to overturning of the structure.

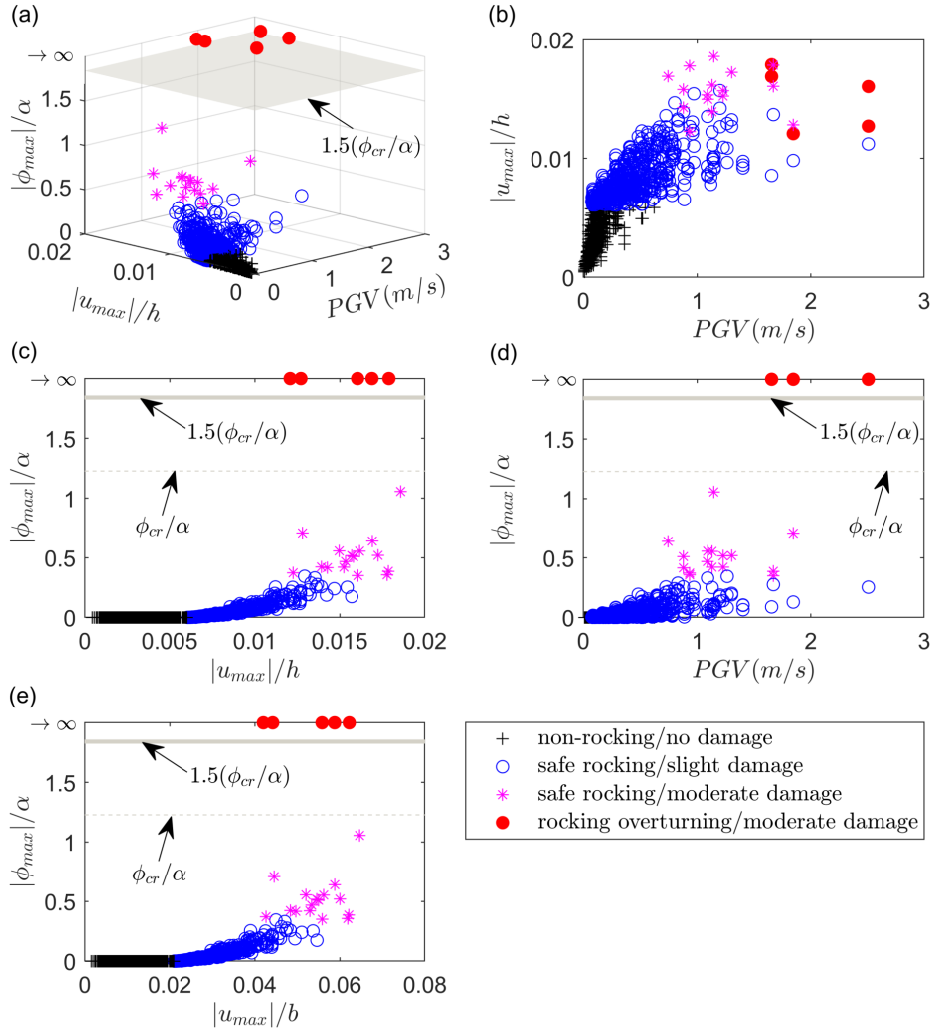


Fig. 6 Seismic response analysis of the rocking structure of Fig. 1(c) (i.e. $\alpha = 0.28$ rad)

3.3 Damage Analysis

The seismic response of e.g. the conventionally designed (fixed-base) **structural system** of Fig. 1(a), investigated in Section 3.2, is related to the damage occurred at the structure through appropriate damage measures. When excessive damage occurs, the structure collapses and subsequently the whole bridge needs to be reconstructed. **This work assumes that damage is occurred only at the column of the structure due to seismic forces [57]; all other kinds of damage (e.g. when impact with the ground occurs after collapse of the structure, etc.) are ignored.** The results from the structural analysis of Fig. 4 are utilized to predict the levels of the expected damage of the fixed-base structure of Fig. 1(a). To quantify the seismic damage, this section adopts the damage limit states (or limit values of column dam-

Table 1 Damage limit states of the conventionally designed (fixed-base) structure of Fig. 1(a).

Damage limit state	Capacity limit [52]	Damage description [49, 16, 44, 57]
LS1	$\frac{ u_{\max} }{h} = 0.005$	<i>Slight</i> concrete cracking and spalling at the column. Onset of yielding of the reinforcing bars. Column in operational condition (damage requires no more than cosmetic repair)
LS2	$\frac{ u_{\max} }{h} = 0.010$	<i>Moderate</i> concrete cracking and spalling at the column. Damage to the exposed reinforcing bars. Minimal residual displacements. Column is still operational (column is structurally sound, damage is repairable)
LS3	$\frac{ u_{\max} }{h} = 0.020$	<i>Extensive</i> flexural damage at the column in the form of buckling and/or fracture of the longitudinal reinforcing bars, transverse steel loss, etc. Considerable residual displacements. Column is not operational (column is structurally unsafe, damage is considerable and repairs are immediate)
LS4	$\frac{ u_{\max} }{h} = 0.025$	<i>Complete</i> damage and collapse of the column (column and the whole bridge need to be reconstructed)

age) proposed by HAZUS [49]. According to HAZUS [49], the damage is categorized into four levels/states, i.e. *slight*, *moderate*, *extensive* and *complete* (Table 1). Jeon et al. [52] proposed drift ratios that quantify each damage limit state of a two-span single-column box-girder bridge constructed in California (e.g. Fig. 1(a)). Specifically, the median column drift ratio limits are 0.5%, 1%, 2% and 2.5% to reach the slight, moderate, extensive and complete damage limit state, respectively. Similar drift ratio limits have also been proposed by [43, 70, 9]. The first damage limit state of 0.5% drift ratio, when exceeded, corresponds to slight cover concrete cracking and spalling at the column end, and it denotes the onset of yielding of the reinforcing bars. However, the column remains in operational condition and the damage requires no more than cosmetic repairs. At the second damage limit state (i.e. 1% drift ratio), damage is described as moderate with the presence of minor residual displacements. The column is still operational and the damage is repairable. Extensive damage occurs when buckling and/or fracture of the reinforcing bars occurs (i.e. at 2% drift ratio). At that damage limit state, the column is structurally unsafe with substantial residual displacements. When the response of the fixed-base structure exceeds the value of 2.5% drift ratio, complete damage and collapse of the column occurs with the reconstruction of the whole bridge to be required.

On the other hand, Figs 5, 6 illustrate that the seismic response of the rocking **structural systems** of Figs 1(b), 1(c), respectively, can be adequately described by three damage limit states (Table 2). The first damage limit state coincides with rocking initiation and occurs when the flexural deformation $|u_{\max}|/h$ becomes equal to the critical deformation u_{cr}/h [95] (i.e. when the condition of Eq. (15) is met). Till that damage limit state, the rocking structures remain in full contact with the ground and, from a dynamics perspective, they behave as single degree-of-freedom (fixed-base) structures. Note that, the limit value of u_{cr}/h of the examined rocking structures is approximately equal to the pertinent limit value of 0.5% drift ratio of the fixed-base **structure** (see e.g. Fig. 4 versus Fig. 5(c) versus Fig. 6(c)). **For this reason and due to the lack of large-scale experiments that quantify the damage accumulated on rocking bridge columns after seismic events, Table 2 assumes that the damage associated with the examined structural systems can be regarded as equivalent when similar drift levels are reached.** Subsequently, after rocking com-

Table 2 Damage limit states of the rocking structures of Figs 1(b), 1(c).

Damage limit state	Capacity limit	Response mode	Damage description
LS1	$\frac{ u_{\max} }{h} = \frac{u_{cr}}{h}$	Rocking initiation	<i>Slight</i> concrete cracking and spalling at the column. Onset of yielding of the reinforcing bars. Column in operational condition (damage requires no more than cosmetic repair)
LS2	$\frac{ \phi_{\max} }{\alpha} = 0.35$	Safe rocking	<i>Moderate</i> concrete cracking and spalling at the column. Damage to the exposed reinforcing bars. Minimal residual displacements. Damage at the pivot points and the abutments due to rocking motion. Column is still operational (column is structurally sound, damage is repairable)
LS3	$\frac{ \phi_{\max} }{\alpha} = 1.5 \left(\frac{\phi_{cr}}{\alpha} \right)$	Rocking overturning	<i>Moderate</i> concrete cracking and spalling at the column. Damage to the exposed reinforcing bars. Minimal residual displacements. Damage at the pivot points and the abutments due to rocking motion. Column is still operational (column is structurally sound, damage is repairable, the column-base system can be reused after the applied repair methods, the whole bridge needs to be reconstructed)

mences, slight cover concrete cracking and spalling occur at the rocking column with the damage being minor that requires no more than cosmetic repairs. Further, Figs 5, 6 show that, when the rotation $|\phi_{\max}|/\alpha$ exceeds a limit value of 0.3–0.4, the flexural deformation $|u_{\max}|/h$ of the column increases rapidly with no particular trend. Hence, the limit value of $|\phi_{\max}|/\alpha = 0.35$ is considered as the second damage limit state. **The threshold value of the second damage limit state is based on engineering judgment and it is selected to be relatively small to express the level of safe rocking action that is targeted in rocking applications. Note from Fig. 5(c) that when the limit value of $|\phi_{\max}|/\alpha = 0.35$ is exceeded, the structural deformation $|u_{\max}|/h$ of the rocking column approximately reaches the pertinent deformation of the fixed-base column that corresponds to 1% lateral drift ratio. Therefore, at that damage limit state, this work assumes that, on average, both rocking structures of Figs 1(b), 1(c) experience equivalent levels of damage with the fixed-base structure of Fig. 1(a), which is characterized by moderate cover concrete cracking and spalling, damage at the reinforcing bars and minor residual displacements. However, the rocking columns of Figs 1(b), 1(c) are still structurally sound and the damage is repairable. Note that, during rocking motion, damage is also concentrated at the pivot points and the abutments. This kind of damage, though, is considered as *local* and it is not taken into account during the damage analysis of the rocking structures. In addition, recent studies proposed construction methodologies which aim to minimize the damage at the pivot points (e.g. [26] among others). The last damage limit state (i.e. LS3) corresponds to overturning of the rocking columns due to excessive rocking rotation. Recall from Section 3.2 and Figs 5, 6 that, when $|\phi_{\max}|/\alpha > 1.5(\phi_{cr}/\alpha)$, the rocking oscillator becomes dynamically unstable and the restoring moment is unable to re-center the structure, thus, overturning occurs. In that case, overturning of the rocking columns lead to overturning of the rocking bridges. Importantly, Figs 5, 6 reveal that, even though overturning occurs and both rocking bridges need to be reconstructed,**

the structural deformation (i.e. drift) of the rocking columns remain low (i.e. $|u_{\max}|/h < 1.8\%$) compared to the pertinent deformation that corresponds to the extensive (i.e. 2%) and/or complete (i.e. 2.5%) damage limit state of the fixed-base column. Hence, even when overturning occurs, due to the low structural deformation and thus minimal seismic damage, both rocking columns can be considered as structurally sound with the damage being characterized as moderate and repairable — one of the main benefits of rocking design. Therefore, the analysis herein assumes that, after the applied repair methods, the rocking column-base systems can be reused reducing considerably the repair cost of the structures — a distinct characteristic of the ABC method.

Based on the description of the damage limit states in Tables 1, 2 and the seismic response of the examined structural systems in Figs 4, 5, 6, this section employs the fragility function fitting method [13] to calculate the probability of exceeding the certain limit values that correspond to each damage limit state. The fitting methodology to calculate the probability of exceedance can be estimated following the *maximum likelihood estimation* (MLE) approach [13]. Note that there are alternative methods to calculate the exceedance probability, e.g. the logistic regression, which is commonly used to predict binary outcomes [71]. However, the logistic regression is consistent with maximum likelihood principles and gives (almost) identical results with the MLE methodology [13]. In general, the MLE method calculates the fragility function parameters ($\hat{\mu}$, $\hat{\beta}$) for which the assumed lognormal distribution (with mean μ and standard deviation β) [42] attains the highest likelihood of producing the observed data. Following [83,42], the likelihood function becomes:

$$L_f = \prod_{i=1}^n (P_{LSi|IM})^{z_i} \cdot (1 - P_{LSi|IM})^{1-z_i} \quad (20)$$

where n denotes the number of damage limit states for each structure and z_i is the binomially distributed variable that equals unity when the pertinent damage limit state is reached and null otherwise. $P_{LSi|IM}$ is the probability of reaching or exceeding the damage limit state i given an $IM = X$ and, in general, is equal to [83,42]:

$$P(\text{demand} \geq LS|X) = \Phi\left(\frac{\ln X - \mu}{\beta}\right) = \frac{1}{2} \left(1 + \text{erf}\left(\frac{\ln X - \mu}{\beta\sqrt{2}}\right)\right) \quad (21)$$

where erf is the error function and $\Phi()$ is the standard normal cumulative distribution function. Hence, the likelihood function takes the following form:

$$L_f = \prod_{i=1}^n \Phi\left(\frac{\ln X_i - \mu}{\beta}\right)^{z_i} \cdot \left(1 - \Phi\left(\frac{\ln X_i - \mu}{\beta}\right)\right)^{1-z_i} \quad (22)$$

where numerical optimization returns the parameters $\hat{\mu}$, $\hat{\beta}$ that maximize the likelihood function [13]:

$$\{\hat{\mu}, \hat{\beta}\} = \max_{\mu, \beta} \prod_{i=1}^n \Phi\left(\frac{\ln X_i - \mu}{\beta}\right)^{z_i} \cdot \left(1 - \Phi\left(\frac{\ln X_i - \mu}{\beta}\right)\right)^{1-z_i} \quad (23)$$

Fig. 7 plots the fragility curves of the examined structural systems of Fig. 1. Note from Fig. 7 that, even though rocking motion considerably reduces structural deformation and therefore damage at the column (see e.g. Fig. 4 versus Fig. 5), it makes the structure vulnerable to excessive rocking rotations and thus overturning. Recall from Section 3.2 that, to avoid biased conclusions, the rocking structure of Fig. 1(b) is intentionally designed with its

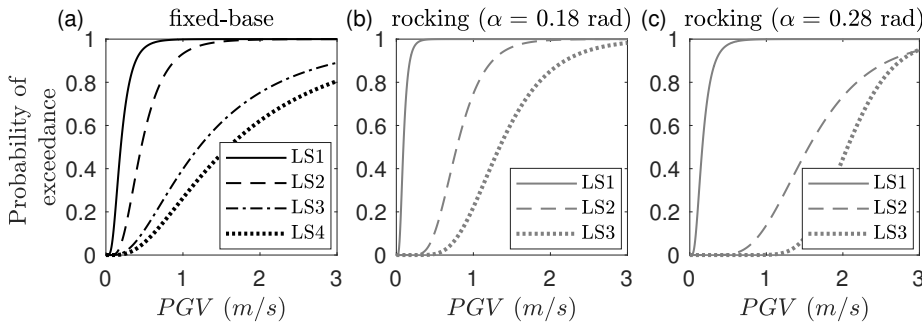


Fig. 7 Fragility curves of (a) the fixed-base structure of Fig. 1(a); and (b), (c) the rocking structures of Figs 1(b), 1(c) with respect to the adopted intensity measure

slenderness outside the optimal range defined in [99], which makes the rocking structure of Fig. 1(b) more fragile with respect to the probability of overturning compared to the probability of collapse of its fixed-base counterpart. **On the other hand, the slenderness of the rocking structure of Fig. 1(c) lies within the optimal range, improving considerably its probability of overturning (as Fig. 7(c) shows).** Nevertheless, a comparison of the structural systems of Fig. 1 solely in terms of their seismic fragility would be unfair and incomplete due to their different structural characteristics and the different nature of the pertinent damage limit states that describe their seismic performance/fragility. For a more holistic approach, more metrics need to be considered. Therefore, this study extends recent studies [99] that focused on the fragility analysis of the structural systems of Fig. 1 and quantifies also their seismic losses expected after severe seismic events.

3.4 Loss Analysis

From the hazard (Section 3.1), structural (Section 3.2) and damage analysis (Section 3.3), the seismic performance of the structural systems of Fig. 1 has been evaluated in terms of response parameters of interest to structural engineers (e.g. rocking rotation and/or flexural deformation). The structural damage, though, investigated in Section 3.3, is related to the seismic losses through decision variables. These decision variables allow engineers, and in general any decision makers, to compare and assess structures in terms of metrics that are comprehensible to all parties. The decision variables considered as the most applicable to bridges are: (i) the (short-term) seismic (repair) losses for the damaged components or the whole bridge [60]; (ii) downtime, i.e. the time that is required for the bridge to restore its functionality through either repair methods or reconstruction of the entire bridge [60,57]; and (iii) resilience, i.e. the ability of the bridge to sustain a level of functionality for over a period of time (determined by the decision makers) [18,19,24,28]. This section translates the seismic response of the examined structural systems investigated in Sections 3.1, 3.2, 3.3 into understandable terms to non-engineers and compares the structures of Fig. 1 in terms of their expected (short-term) seismic losses (see Fig. 8 later on) and their expected long-term seismic losses (see Figs 9, 10 later on) in the aftermath of various seismic hazard scenarios.

Given the fragility curves of Fig. 7, the probability of each structural system to be in the different damage limit states can be computed. Based on the total probability theorem, the seismic losses are defined as the sum of the seismic consequences (e.g. damage and subsequently repair cost) weighted with their probability of occurrence. Therefore, the expected

Table 3 Repair cost ratio and downtime values for each damage limit state of the conventionally designed (fixed-base) structure of Fig. 1(a).

Damage limit state	Repair cost ratio [49]	Repair methods description [44,57]	Downtime (days) [49]	
			Mean	Standard deviation
LS1	0.03	Repair slight concrete cracking/spalling at the column (epoxy injection, patch with concrete, etc.)	0.6	0.6
LS2	0.08	Repair moderate concrete cracking/spalling at the column, repair damaged reinforcing bars (patch with concrete, reinforce and recast, etc.)	2.5	2.7
LS3	0.25	Repair extensive concrete cracking/spalling at the column, replace/repair longitudinal/transverse reinforcing bars (reinforce and recast, potential replacement of the column)	75	42
LS4	1	Demolition and reconstruction of the column and the whole bridge	230	110

seismic losses under the given IM can be expressed as [39]:

$$E(l) = \sum_{i=1}^n C_i \cdot P_{LSi|IM} \quad (24)$$

where C_i represents the seismic consequences, e.g. the repair cost associated with the given damage limit state i , and $P_{LSi|IM}$ is the conditional probability of the structure to be at the given damage limit state. The consequences of a seismic event C_i are quantified in monetary values and expressed as the summation of the direct and indirect costs accumulated after an earthquake. Direct costs are usually associated with the reconstruction expenses and are directly related to the level of structural damage. Indirect costs account for the losses caused by additional travel time and distance (e.g. when the bridge is partially or fully closed) [84,59,28]. This work considers only the direct costs. Therefore, the seismic consequences (i.e. direct costs) associated with the given damage limit states are assumed proportional to the reconstruction cost of the bridge [84,63,28,39]:

$$C_i = RCR_i \cdot c_{rec} \cdot W \cdot L \quad (25)$$

where W and L are the bridge width and length, respectively. c_{rec} is the reconstruction cost, which for the fixed-base structure of Fig. 1(a) is translated into $2,306 \text{ \$/m}^2$ in present monetary values [101]. RCR_i is the repair cost ratio that corresponds to each damage limit state. The repair cost ratios are expressed as a percentage of the reconstruction cost of the entire bridge [49], and they differ from damage limit state to damage limit state since the repair methods vary depending on the magnitude of damage. In particular, low levels of damage (i.e. 0.5% drift ratio in Table 1) cause cover concrete cracking and spalling, which can be repaired using concrete patching, epoxy crack sealing, etc. (Table 3). Higher levels of damage (i.e. 1% drift ratio in Table 1) require replacement of the buckled reinforcing bars, steel jacketing or even replacement of the column in case it is considered as structurally unsafe (i.e. 2% drift ratio in Table 1). Hence, the more severe the damage, the larger the repair cost ratio. HAZUS [49] proposed repair cost ratio values for conventionally designed (fixed-base) bridges (Table 3). Note in Table 3 that, in case of bridge collapse (i.e. when LS4

Table 4 Repair cost ratio and downtime values for each damage limit state of the rocking structures of Figs 1(b), 1(c).

Damage limit state	Repair cost ratio [49]	Repair methods description	Downtime (days) [49,64]	
			Mean	Standard deviation
LS1	0.03	Repair slight concrete cracking/spalling at the column (epoxy injection, patch with concrete, etc.)	0.6	0.6
LS2	0.08	Repair moderate concrete cracking/spalling at the column, repair damaged reinforcing bars (patch with concrete, reinforce and recast, etc.). Repair damage at the pivot points and the abutments	2.5	2.7
LS3	1	Repair moderate concrete cracking/spalling at the column, repair damaged reinforcing bars (patch with concrete, reinforce and recast, etc.). Repair damage at the pivot points and the abutments. Reuse the column-base system after the applied repair methods. Reconstruction of the whole bridge	46	22

in Table 1 is exceeded), the repair cost equals the reconstruction cost of the bridge, thus, the repair cost ratio becomes unity.

Similarly, Table 4 presents the pertinent repair cost ratio values for each damage limit state of the rocking structures of Figs 1(b), 1(c). Importantly, recall that, uplift considerably reduces structural deformation (i.e. drift) and therefore the accumulated (on the column) seismic damage (see e.g. Fig. 4 versus Fig. 5). In addition, even when overturning occurs, the rocking columns, **due to low drift levels**, are still structurally sound and the damage is moderate and repairable. Hence, the rocking column-base systems after the applied repair methods can be reused, reducing considerably the repair costs of the structures (see e.g. Section 3.3). To capture the decrease on the repair cost of a rocking structure, Marriott et al. [65] assigned lower values of repair cost ratios to each damage limit state of the examined rocking bridges compared to the pertinent values of the fixed-base bridge. In contrast, due to the lack of adequate large-scale experiments that focus on the accumulated seismic damage on rocking bridge columns, this work introduces the coefficient r to quantify the decrease on the repair cost in the aftermath of seismic events. In particular, since the seismic damage accumulated on the column of the rocking structures is less severe than the pertinent damage on the column of the fixed-base structure (see e.g. Fig. 4 versus Fig. 5), $0 < r < 1$. For instance, $r = 0.5$ implies that the seismic consequences on the rocking structure are half of the pertinent consequences on the fixed-base structure. However, this does not mean that the corresponding seismic losses are similarly half, since the expected seismic losses are also related to the probability of occurrence of the pertinent seismic consequences (see e.g. Eq. (24)). Subsequently, for the case of the rocking structures of Figs 1(b), 1(c), Eq. (25) can be re-written as:

$$C_i = RCR_i \cdot r \cdot c_{rec} \cdot W \cdot L \quad (26)$$

To assess the expected seismic losses of the examined structures, this study considers nine different seismic hazard scenarios. These scenarios correspond to seismic events with $T_R = 40, 72, 125, 225, 475, 975, 1,485, 2,475$ and $4,975$ -year return period, which translate into a probability of 71%, 50%, 33%, 20%, 10%, 5%, 3%, 2% and 1%, respectively, that at least one such event will occur in the next 50 years in the area of focus. **Note that this**

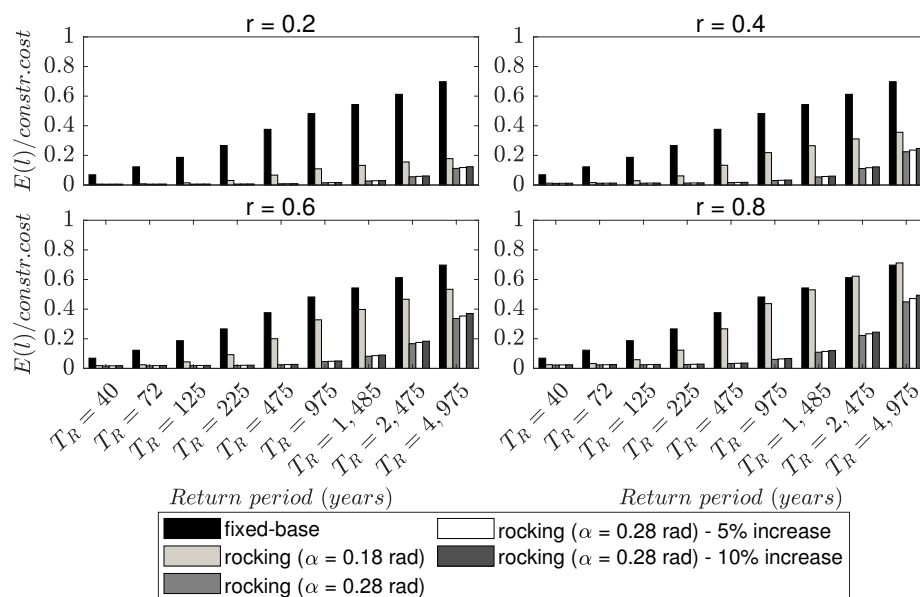


Fig. 8 Expected (short-term) seismic losses normalized with respect to the construction cost of the fixed-base structure of Fig. 1(a) in the aftermath of various seismic hazard scenarios

work assumes that these seismic events are independent of each other. The hazard curve of Fig. 3(b) provides the intensities in terms of PGV values that correspond to the adopted seismic hazard scenarios, i.e. 0.37, 0.51, 0.65, 0.83, 1.08, 1.36, 1.53, 1.76 and 2.11 m/s, respectively. Therefore, given the fragility curves (Fig. 7) and the repair cost ratios for each damage limit state (Tables 3, 4), the expected seismic losses can be computed.

Fig. 8 presents a comparison of the examined structural systems in terms of the expected seismic losses accumulated after the considered seismic hazard scenarios. To generalize the results, Fig. 8 is presented in dimensionless terms normalized with respect to the construction cost of the fixed-base structure of Fig. 1(a) (i.e. $2,306 \text{ \$/m}^2$ [101]), which is the same as the construction cost of the rocking structure of Fig. 1(b) since both structures have identical geometry and are made of the same material. Observe that, due to the larger base-width, the geometry of the rocking structure of Fig. 1(c) is slightly different from the geometry of e.g. the rocking structure of Fig. 1(b). Fig. 8 illustrates the effect of the difference in geometry of the examined structural systems on the seismic losses assuming that the construction cost of the rocking structure of Fig. 1(c) either remains the same as e.g. the construction cost of the fixed-base structure of Fig. 1(a), or, due to its larger base-width, is 5% or 10% increased. Note that the difference in the geometry of the structure of Fig. 1(c) is small, thus, the increase of its construction cost can be adequately captured by either the 5% or (even) the 10% increase. As a first approach, Fig. 8 shows that the difference in the geometry of the structure of Fig. 1(c) has minimal effect on its seismic losses. In addition, Fig. 8 reveals that, for almost all of the examined seismic hazard scenarios, the rocking structure of Fig. 1(b) provides a significant post-earthquake financial benefit compared to its fixed-base counterpart. Observe that, only after extreme seismic events with $T_R = 2,475$ and $4,975$ -year return period and only when $r = 0.8$, which practically means that the repair cost of the rocking structure of Fig. 1(b) is 80% of the repair cost of the fixed-base structure of Fig. 1(a), the

rocking structure returns equivalent seismic losses compared to the fixed-base structure. The occurrence rate of such seismic events, though, is only 2% and 1%, respectively, in the next 50 years. For more frequent seismic events, the rocking structure outweighs the fixed-base structure with considerably lower seismic losses regardless of the cost for the repairs (i.e. the exact value of r). **Importantly, note from Fig. 8 that when the rocking structure is carefully designed (i.e. Fig. 1(c)), its seismic losses are substantially mitigated. In particular, even after a severe seismic event (i.e. with $T_R = 4,975$ -year return period) and even when $r = 0.8$, the rocking structure of Fig. 1(c) yields seismic losses which correspond to less than 50% of the construction cost of the bridge. After less severe seismic events (i.e. with $T_R = 40, 72, 125, 225, 475, 975, 1,485$ and $2,475$ -year return period), regardless of the cost for the repairs (i.e. the exact value of r), its seismic losses are consistently lower than 25% of the construction cost of the bridge — a considerable post-earthquake financial benefit.** A further decrease on the expected seismic losses of the rocking structures of Figs 1(b), 1(c) can be achieved by enhancing their seismic performance, thus, reducing their seismic fragility (Fig. 7) through the use of e.g. additional re-centering and/or energy dissipation capacity, increasing in that way, though, their construction cost. However, such an analysis merits further investigation, which is beyond the scope of the present study.

Assuming the earthquake occurrence as a Poisson process with an occurrence rate of λ_M , the expected long-term seismic losses can be expressed as [96,97]:

$$E(L_{LC}) = \frac{\lambda_M \cdot E(l)}{\gamma} (1 - e^{-\gamma t_{int}}) \quad (27)$$

where t_{int} is the investigated time-interval (in years) and γ is the monetary discount rate equal to 0.02. Fig. 9 plots the expected long-term seismic losses normalized with respect to the construction cost of the fixed-base structure of Fig. 1(a). For brevity, Fig. 9 considers two seismic hazard scenarios: (i) a design earthquake (i.e. with $T_R = 475$ -year return period and 10% probability of occurrence in the next 50 years) (Fig. 9(a)); and (ii) a maximum considered earthquake (i.e. with $T_R = 2,475$ -year return period and 2% probability of occurrence in the next 50 years) (Fig. 9(b)). As a first approach, Fig. 9 verifies the results of Fig. 8. Specifically, Fig. 9 shows that, after a design earthquake, both rocking structures of Figs 1(b), 1(c) yield lower long-term seismic losses than the fixed-base structure of Fig. 1(a) regardless of the cost for the repairs (i.e. the exact value of r). **Further, after a maximum considered earthquake, the long-term seismic losses of the rocking structure of Fig. 1(b) become equivalent with the pertinent losses of the fixed-base structure of Fig. 1(a) only when the repair cost of the rocking structure is 80% of the repair cost of the fixed-base structure (i.e. when $r = 0.8$) (see also Fig. 8). On the contrary, the rocking structure of Fig. 1(c) consistently outweighs both the fixed-base structure of Fig. 1(a) and the rocking structure of Fig. 1(b), which verifies that a rocking bridge when it is carefully designed provides a significant post-earthquake financial benefit.** In addition, note in Fig. 9 that a higher intensity earthquake (i.e. with $T_R = 2,475$ -year return period) yields lower long-term seismic losses than a lower intensity earthquake (i.e. with $T_R = 475$ -year return period). This counter-intuitive conclusion is due to the lower rate of occurrence (i.e. λ_M in Eq. (27)) of higher intensity earthquakes compared to the corresponding rate of occurrence of lower intensity earthquakes.

In the same context, Fig. 10 presents the (cumulative) long-term losses of all nine seismic hazard scenarios with $T_R = 40, 72, 125, 225, 475, 975, 1,485, 2,475$ and $4,975$ -year return period weighted with their probability of occurrence. Comparison of Figs 9, 10 verifies that increasing the number of the seismic events that would occur in the area of focus, the

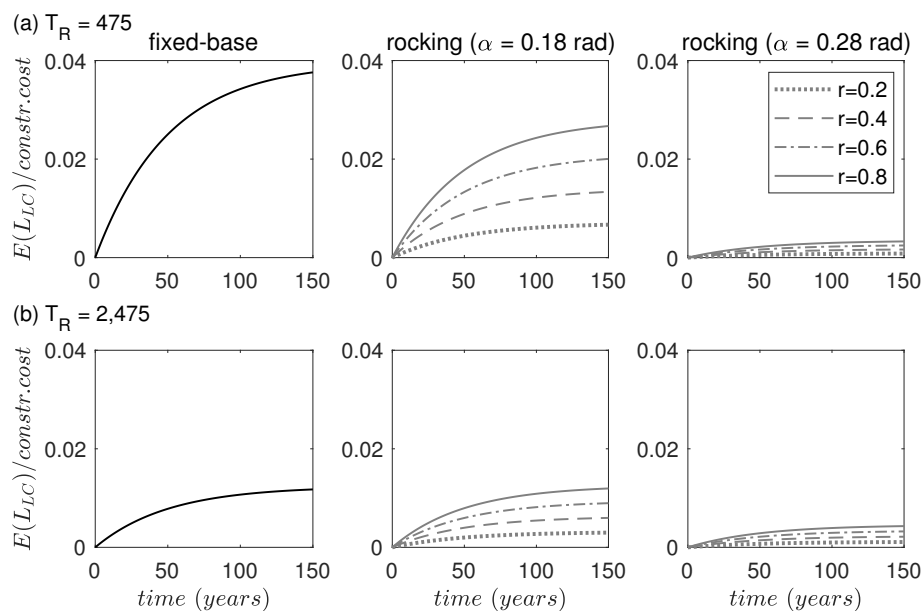


Fig. 9 Expected long-term seismic losses normalized with respect to the construction cost of the fixed-base structure of Fig. 1(a) of (a) a design earthquake (i.e. with $T_R = 475$ -year return period and 10% probability of occurrence in the next 50 years); and (b) a maximum considered earthquake (i.e. with $T_R = 2,475$ -year return period and 2% probability of occurrence in the next 50 years)

(cumulative) long-term seismic losses would increase. However, further increase of the considered seismic events would jeopardize the assumption of their independence among each other. Hence, such an analysis is ignored. Further, Fig. 10 reveals the substantially lower long-term seismic losses of both rocking structures compared to their fixed-base counterpart regardless of the cost for the repairs (i.e. the exact value of r). In addition, Fig. 10(c) highlights how cost-efficient a rocking structure can be in the long-term when it is carefully designed.

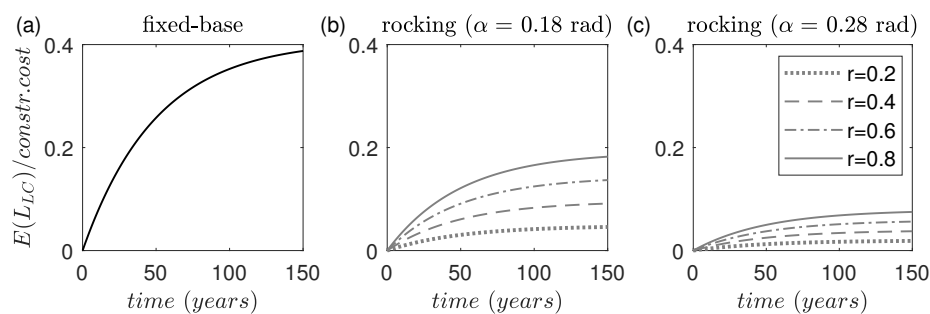


Fig. 10 Expected (cumulative) long-term seismic losses normalized with respect to the construction cost of the fixed-base structure of Fig. 1(a) of nine seismic hazard scenarios (i.e. with $T_R = 40, 72, 125, 225, 475, 975, 1,485, 2,475$ and $4,975$ -year return period and 71%, 50%, 33%, 20%, 10%, 5%, 3%, 2% and 1% probability of occurrence in the next 50 years, respectively)

In sum, Figs 8, 9, 10 reveal the considerable post-earthquake financial benefits that a rocking structure provides, illustrating its dominance over the conventionally designed (fixed-base) structure. In addition, Figs 8, 9, 10 highlight that a more careful design of a rocking structure can further decrease its (short-term and long-term) seismic losses. In addition, Section 3.4 also underlines the need for large-scale experiments that quantify the damage accumulated at the column of the structure during rocking motion and propose pertinent repair cost ratios for each damage limit state.

4 From Performance-Based to Resilience-Based Earthquake Engineering Assessment of Single-Column Rocking Bridges

The performance-based earthquake engineering (PBEE) framework, adopted in Section 3, evaluates the seismic performance of a structural system in terms of target demands (e.g. peak drift and/or peak rotation). However, the PBEE approach does not incorporate the post-earthquake functionality and resilience of the structure, which are also important indicators of its seismic performance. On the other hand, the *resilience-based earthquake engineering* (RBEE) framework focuses on mitigating the earthquake-induced risks to enable rapid recovery of the structure in the aftermath of severe earthquakes. Therefore, the RBEE appears to be a more holistic approach and it is considered as an extension of the PBEE in the design process (see e.g. [6, 25] for a more detailed analysis).

Resilience represents the ability of the structure to recover from a damaged condition to the pre-damaged functionality level. Specifically, as a performance indicator, it quantifies the recovery (or restoration) functions of a structural system following a seismic event. These recovery functions depend on the associated damage limit states. For instance, a bridge completely damaged needs more time to restore its functionality compared to a slightly damaged bridge. In general, after an earthquake, repair methods are applied to the damaged structure and its functionality starts to increase (with respect to time) up to a desirable level [59]. Various analytical models have been proposed to capture the restoration process using e.g. linear, stepwise [73], exponential [53], trigonometric [20] or cumulative distribution functions [8, 49]. This study models the functionality restoration (FR) process of each structure of Fig. 1 as a normal cumulative distribution function corresponding to each damage limit state i [8, 49]:

$$FR_i(t) = \frac{1}{2} \left[1 + \operatorname{erf} \left(\frac{t - \mu_{d_i}}{\sqrt{2}\sigma_{d_i}} \right) \right] \quad (28)$$

where μ_{d_i} and σ_{d_i} represent the mean and standard deviation of the time during which the bridge is under restoration (i.e. downtime). HAZUS [49] proposed appropriate mean and standard deviation values of downtime (in days) depending on the level of damage and thus the appropriate repair methods. Table 3 presents these values for the fixed-base structure of Fig. 1(a). To estimate the corresponding downtime values for a rocking structure (e.g. Figs 1(b), 1(c)), Mantawy et al. [64] experimentally compared the seismic performance of a rocking versus a conventionally designed (fixed-base) bridge. That study showed, among others, that the construction time of the rocking bridge is, on average, 5 times lower than the construction time of the fixed-base bridge. In other words, when the fixed-base and the rocking structures of Fig. 1 need to be reconstructed (i.e. when LS4 in Table 3 and LS3 in Table 4 are exceeded), the downtime of the rocking structures is considered as 1/5 of the downtime of the fixed-base structure. Table 4 presents the pertinent mean and standard deviation values of downtime for the rocking structures of Figs 1(b), 1(c). Note that the

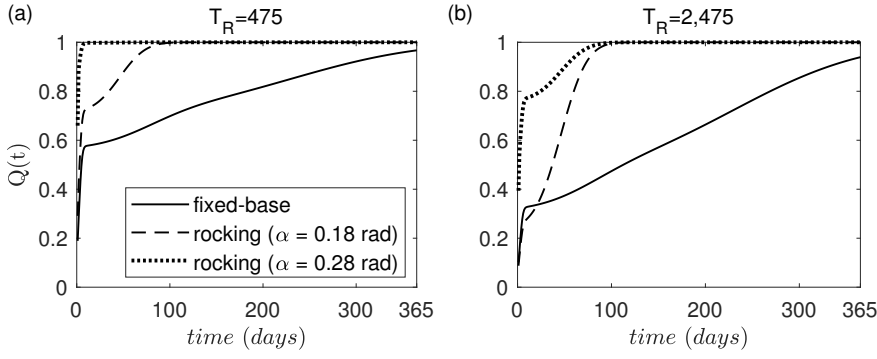


Fig. 11 Expected functionality of the examined structures in the aftermath of (a) a design earthquake (i.e. with $T_R = 475$ -year return period and 10% probability of occurrence in the next 50 years); and (b) a maximum considered earthquake (i.e. with $T_R = 2,475$ -year return period and 2% probability of occurrence in the next 50 years)

remaining downtime values are identical among the structures of Fig. 1 (see Table 3 versus Table 4) since damage is considered equivalent (see “damage description” in Tables 1, 2).

Based on the functionality restoration models applied to the structure after a seismic event (e.g. Eq. (28)), its functionality can be quantified by mapping each damage limit state to a value between null and unity. For instance, functionality equals to unity indicates that the structure is completely functional, whereas functionality equals to null denotes a completely damaged structure. Therefore, the expected (dimensionless) time-variant functionality $Q(t)$ can be expressed as [73, 38]:

$$Q(t) = \sum_{i=1}^n FR_i(t) \cdot P_{LSi|IM} \quad (29)$$

Fig. 11 plots the expected functionality of the examined structural systems in the aftermath of a design earthquake (i.e. with $T_R = 475$ -year return period and 10% probability of occurrence in the next 50 years) (Fig. 11(a)) and a maximum considered earthquake (i.e. with $T_R = 2,475$ -year return period and 2% probability of occurrence in the next 50 years) (Fig. 11(b)). In Fig. 11, $time = t_0 = 0$ (days) denotes the time-instant the seismic event occurs. Fig. 11 reveals the remarkable post-earthquake functionality of both rocking structures compared to the fixed-base structure. Observe that, after a maximum considered earthquake (Fig. 11(b)), both rocking structures restore their functionality in less than 1/3 of the time needed for their fixed-base counterpart to reach equivalent levels of functionality. **After a design earthquake (Fig. 11(a)), a rocking structure restores its functionality almost immediately when it is carefully designed.** Importantly, the dominance of the rocking structures is consistent under all the remaining seismic hazard scenarios examined herein (i.e. with $T_R = 40, 72, 125, 225, 975, 1,485$ and 4,975-year return period). For brevity, though, those results are omitted.

Given the time-variant post-earthquake functionality of Eq. (29), the resilience of the structural systems of Fig. 1 can be quantified under the investigated time-interval (i.e. $\Delta t = 365$ days). Specifically, the resilience can be expressed as [18, 19, 24]:

$$R = \frac{1}{\Delta t} \int_{t_0}^{t_0 + \Delta t} Q(t) dt \quad (30)$$

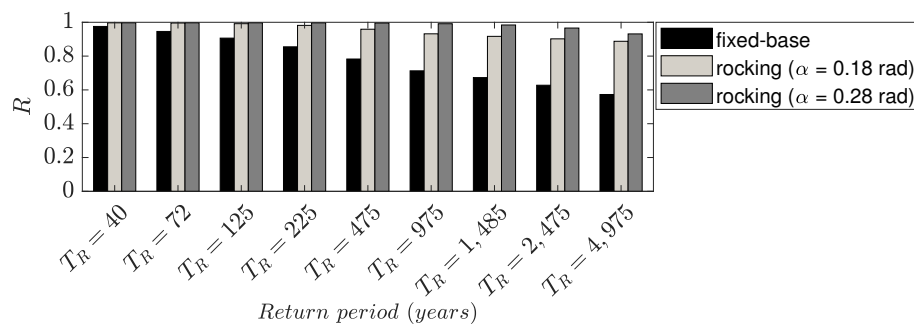


Fig. 12 Resilience of the examined structures in the aftermath of various seismic hazard scenarios under the investigated time-interval of $\Delta t = 365$ days

where t_0 indicates the time-instant the seismic event occurs. Similarly, the resilience is a dimensionless parameter that is quantified with values between null and unity; the closer to unity, the more resilient the structure. Fig. 12 illustrates the dominance of the rocking structures over the conventionally designed (fixed-base) structure after all the examined seismic hazard scenarios. Note that the resilience of the rocking structure of Fig. 1(b) starts deteriorating only when a design earthquake occurs (i.e. with $T_R = 475$ -year return period). **Importantly, the resilience of the rocking structure of Fig. 1(c) starts decreasing only when a maximum considered earthquake occurs (i.e. with $T_R = 2,475$ -year return period).** On the contrary, the resilience of the fixed-base structure of Fig. 1(a) is impaired even when a low intensity earthquake occurs (i.e. with $T_R = 72$ -year return period).

In sum, Figs 11, 12 reveal the remarkable post-earthquake functionality and resilience of the examined rocking structures in the aftermath of severe seismic hazard scenarios. **Further, both Figs 11, 12 underline the importance of a careful design of a rocking structure highlighting that even a small modification of its slenderness can lead to substantial post-earthquake financial benefits.**

5 Conclusions

This work investigates the seismic performance of structural systems, which are particularly attractive for bridge design. It focuses on single-column bridges either monolithically connected with the ground (i.e. fixed-base) or able to uplift and exhibit planar rocking motion during an earthquake. It employs the well-established performance-based earthquake engineering (PBEE) framework to compare the examined structural systems in terms of their seismic fragility and the accumulated seismic losses in the aftermath of severe seismic hazard scenarios. In addition, the present study extends the PBEE approach to evaluate the post-earthquake functionality and resilience of the examined structures adopting a more holistic resilience-based earthquake engineering framework.

The analysis reveals the considerably mitigated (short-term and long-term) seismic losses of the examined rocking structures compared to the pertinent losses of the fixed-base structure, illustrating their potential as an economically feasible design solution. In particular, even for a rocking structure, which is intentionally designed to be more fragile with respect to the probability of overturning compared to the probability of collapse of its fixed-base counterpart, only after extreme seismic events (i.e. with $T_R = 2,475$ and 4,975-year return period, which translate into 2% and 1% probability of occurrence in the next 50 years,

respectively) and only when the repair cost of the rocking structure is 80% of the the repair cost of the fixed-base structure, the rocking structure returns equivalent seismic losses compared to the pertinent losses of the fixed-base structure. In all the remaining seismic hazard scenarios examined herein, the rocking structure outweighs the fixed-base structure (in terms of seismic losses) regardless of the cost for the repairs of the structural systems. **Importantly, the results show that even a small modification of the slenderness of the rocking structure can yield substantially lower seismic losses compared to its fixed-base counterpart regardless of the considered seismic event and/or the cost for the repairs — highlighting the importance of a careful design.**

Further, this paper also unveils the remarkable post-earthquake functionality and resilience of the examined rocking structures after various seismic hazard scenarios. Specifically, after a maximum considered earthquake (i.e. with $T_R = 2,475$ -year return period and 2% probability of occurrence in the next 50 years), both rocking structures restore their functionality in less than 1/3 of the time needed for their fixed-base counterpart to reach equivalent levels of functionality. **Note that after a design earthquake (i.e. with $T_R = 475$ -year return period and 10% probability of occurrence in the next 50 years), the functionality of the rocking structure is substantially enhanced when it is carefully designed.** In addition, the results show that a rocking structure sustains its resilience at the highest level till a design earthquake occurs (i.e. with $T_R = 475$ -year return period and 10% probability of occurrence in the next 50 years). **Importantly, even a small modification of its slenderness can yield a rocking structure that sustains its resilience at the highest level till a maximum considered earthquake occurs (i.e. with $T_R = 2,475$ -year return period and 2% probability of occurrence in the next 50 years).** On the contrary, the resilience of the fixed-base structure is deteriorated even when a low intensity earthquake occurs (i.e. with $T_R = 72$ -year return period and 50% probability of occurrence in the next 50 years). The above findings redirect our attention to the main post-earthquake financial benefits of rocking design when used as a seismic isolation technique for bridges and pave the way for a more rational and holistic seismic assessment framework of single-column rocking bridges.

Acknowledgements This study has been supported by the National Natural Science Foundation of China (Grant No. 51808476), and the Chinese National Engineering Research Centre (CNERC) for Steel Construction (Hong Kong Branch) at the Hong Kong Polytechnic University (Project No. P0006216). Their support is gratefully acknowledged. The opinions and conclusions presented in this paper are those of the authors and do not necessarily reflect the views of the sponsoring organizations.

References

1. Acikgoz, S., DeJong, M.J.: The interaction of elasticity and rocking in flexible structures allowed to uplift. *Earthquake Engineering & Structural Dynamics* **41**(15), 2177–2194 (2012)
2. Acikgoz, S., DeJong, M.J.: Analytical modelling of multi-mass flexible rocking structures. *Earthquake Engineering & Structural Dynamics* **45**(13), 2103–2122 (2016)
3. Acikgoz, S., DeJong, M.J.: Vibration modes and equivalent models for flexible rocking structures. *Bulletin of Earthquake Engineering* **15**(10), 4427–4452 (2017)
4. Acikgoz, S., Ma, Q., Palermo, A., DeJong, M.J.: Experimental identification of the dynamic characteristics of a flexible rocking structure. *Journal of Earthquake Engineering* **20**(8), 1199–1221 (2016)
5. Agalianos, A., Psychari, A., Vassiliou, M.F., Stojadinovic, B., Anastasopoulos, I.: Comparative assessment of two rocking isolation techniques for a motorway overpass bridge. *Frontiers in Built Environment* **3**, 47 (2017)
6. Almufti, I., Willford, M.: REDi™ rating system: Resilience-based earthquake design initiative for the next generation of buildings, version 1.0. Tech. rep., Arup (2013)

7. Antonellis, G., Panagiotou, M.: Seismic response of bridges with rocking foundations compared to fixed-base bridges at a near-fault site. *Journal of Bridge Engineering* **19**(5), 04014007 (2014)
8. ATC: Earthquake damage evaluation data for California. Tech. Rep. ATC-13, Applied Technology Council, Redwood City, CA (1985)
9. Babazadeh, A., Burgueño, R., Silva, P.F.: Use of 3D finite-element models for predicting intermediate damage limit states in RC bridge columns. *Journal of Structural Engineering* **141**(10), 04015012 (2015)
10. Bachmann, J.A., Strand, M., Vassiliou, M.F., Broccardo, M., Stojadinovic, B.: Is rocking motion predictable? *Earthquake Engineering & Structural Dynamics* **47**(2), 535–552 (2018)
11. Bachmann, J.A., Vassiliou, M.F., Stojadinovic, B.: Dynamics of rocking podium structures. *Earthquake Engineering & Structural Dynamics* **46**(14), 2499–2517 (2017)
12. Bachmann, J.A., Vassiliou, M.F., Stojadinovic, B.: Rolling and rocking of rigid uplifting structures. *Earthquake Engineering & Structural Dynamics* **48**(14), 1556–1574 (2019)
13. Baker, J.W.: Efficient analytical fragility function fitting using dynamic structural analysis. *Earthquake Spectra* **31**(1), 579–599 (2015)
14. Baker, J.W.: An introduction to probabilistic seismic hazard analysis. White Paper Version 2.1 **2**(1), 79 (2015)
15. Baker, J.W., Lin, T., Shahi, S.K., Jayaram, N.: New ground motion selection procedures and selected motions for the peer transportation research program. Tech. Rep. PEER Report 2011/3, Pacific Earthquake Engineering Research Center, University of California, Berkeley, CA (2011)
16. Basöz, N.I., Kiremidjian, A.S., King, S.A., Law, K.H.: Statistical analysis of bridge damage data from the 1994 Northridge, CA, earthquake. *Earthquake Spectra* **15**(1), 25–54 (1999)
17. Boore, D.M., Stewart, J.P., Seyhan, E., Atkinson, G.M.: NGA-WEST2 equations for predicting PGA, PGV, and 5% damped PSA for shallow crustal earthquakes. *Earthquake Spectra* **30**(3), 1057–1085 (2014)
18. Bruneau, M., Chang, S.E., Eguchi, R.T., Lee, G.C., O'Rourke, T.D., Reinhorn, A.M., Shinozuka, M., Tierney, K., Wallace, W.A., Von Winterfeldt, D.: A framework to quantitatively assess and enhance the seismic resilience of communities. *Earthquake Spectra* **19**(4), 733–752 (2003)
19. Bruneau, M., Reinhorn, A.: Exploring the concept of seismic resilience for acute care facilities. *Earthquake Spectra* **23**(1), 41–62 (2007)
20. Chang, S.E., Shinozuka, M.: Measuring improvements in the disaster resilience of communities. *Earthquake Spectra* **20**(3), 739–755 (2004)
21. Chen, Y., Larkin, T., Chou, N.: Experimental assessment of contact forces on a rigid base following footing uplift. *Earthquake Engineering & Structural Dynamics* **46**(11), 1835–1854 (2017)
22. Chopra, A.K.: *Dynamics of structures*, vol. 3. Prentice Hall New Jersey (1995)
23. Chopra, A.K., Yim, S.C.S.: Simplified earthquake analysis of structures with foundation uplift. *Journal of Structural Engineering* **111**(4), 906–930 (1985)
24. Cimellaro, G.P., Reinhorn, A.M., Bruneau, M.: Framework for analytical quantification of disaster resilience. *Engineering Structures* **32**(11), 3639–3649 (2010)
25. Cimellaro, G.P., Renschler, C., Bruneau, M.: Introduction to resilience-based design (RBD). In: *Computational Methods, Seismic Protection, Hybrid Testing and Resilience in Earthquake Engineering*, pp. 151–183. Springer (2015)
26. Cui, H., Wu, G., Zhang, J., Xu, J.: Experimental study on damage-controllable rocking walls with resilient corners. *ICE Magazine of Concrete Research* pp. 1–17 (2019)
27. Dar, A., Konstantinidis, D., El-Dakhkhni, W.: Seismic response of rocking frames with top support eccentricity. *Earthquake Engineering & Structural Dynamics* **47**(12), 2496–2518 (2018)
28. Decò, A., Bocchini, P., Frangopol, D.M.: A probabilistic approach for the prediction of seismic resilience of bridges. *Earthquake Engineering & Structural Dynamics* **42**(10), 1469–1487 (2013)
29. DeJong, M.J., Dimitrakopoulos, E.G.: Dynamically equivalent rocking structures. *Earthquake Engineering & Structural Dynamics* **43**(10), 1543–1563 (2014)
30. Di Egidio, A., Contento, A.: Base isolation of slide-rocking non-symmetric rigid blocks under impulsive and seismic excitations. *Engineering Structures* **31**(11), 2723–2734 (2009)
31. Di Sarno, L., Magliulo, G., D'Angela, D., Cosenza, E.: Experimental assessment of the seismic performance of hospital cabinets using shake table testing. *Earthquake Engineering & Structural Dynamics* **48**(1), 103–123 (2019)
32. Diamantopoulos, S., Fragiadakis, M.: Seismic response assessment of rocking systems using single degree-of-freedom oscillators. *Earthquake Engineering & Structural Dynamics* **48**(7), 689–708 (2019)
33. Dimitrakopoulos, E.G., DeJong, M.J.: Overturning of retrofitted rocking structures under pulse-type excitations. *Journal of Engineering Mechanics* **138**(8), 963–972 (2012)
34. Dimitrakopoulos, E.G., DeJong, M.J.: Revisiting the rocking block: closed-form solutions and similarity laws. *Proceedings of the Royal Society A: Mathematical, Physical and Engineering Science* **468**(2144), 2294–2318 (2012)

35. Dimitrakopoulos, E.G., Fung, E.D.W.: Closed-form rocking overturning conditions for a family of pulse ground motions. *Proceedings of the Royal Society A: Mathematical, Physical and Engineering Science* **472**(2196), 20160662 (2016)
36. Dimitrakopoulos, E.G., Giouvanidis, A.I.: Seismic response analysis of the planar rocking frame. *Journal of Engineering Mechanics* **141**(7), 04015003 (2015)
37. Dimitrakopoulos, E.G., Paraskeva, T.S.: Dimensionless fragility curves for rocking response to near-fault excitations. *Earthquake Engineering & Structural Dynamics* **44**(12), 2015–2033 (2015)
38. Dong, Y., Frangopol, D.M.: Risk and resilience assessment of bridges under mainshock and aftershocks incorporating uncertainties. *Engineering Structures* **83**, 198–208 (2015)
39. Dong, Y., Frangopol, D.M., Saydam, D.: Time-variant sustainability assessment of seismically vulnerable bridges subjected to multiple hazards. *Earthquake Engineering & Structural Dynamics* **42**(10), 1451–1467 (2013)
40. Fajfar, P., Krawinkler, H.: *Seismic design methodologies for the next generation of codes*. Taylor & Francis (1997)
41. Fardis, M.N.: Uplift of deck or footings in bridges with distributed mass subjected to transverse earthquake. *Earthquake Engineering & Structural Dynamics* **44**(15), 2755–2773 (2015)
42. Gehl, P., Seyedi, D.M., Douglas, J.: Vector-valued fragility functions for seismic risk evaluation. *Bulletin of Earthquake Engineering* **11**(2), 365–384 (2013)
43. Ghobarah, A.: Performance-based design in earthquake engineering: state of development. *Engineering Structures* **23**(8), 878–884 (2001)
44. Ghosh, J., Padgett, J.E.: Probabilistic seismic loss assessment of aging bridges using a component-level cost estimation approach. *Earthquake Engineering & Structural Dynamics* **40**(15), 1743–1761 (2011)
45. Giouvanidis, A.I., Dimitrakopoulos, E.G.: Nonsmooth dynamic analysis of sticking impacts in rocking structures. *Bulletin of Earthquake Engineering* **15**(5), 2273–2304 (2017)
46. Giouvanidis, A.I., Dimitrakopoulos, E.G.: Seismic performance of rocking frames with flag-shaped hysteretic behavior. *Journal of Engineering Mechanics* **143**(5), 04017008 (2017)
47. Giouvanidis, A.I., Dimitrakopoulos, E.G.: Rocking amplification and strong-motion duration. *Earthquake Engineering & Structural Dynamics* **47**(10), 2094–2116 (2018)
48. Gutenberg, B., Richter, C.F.: Frequency of earthquakes in California. *Bulletin of the Seismological Society of America* **34**(4), 185–188 (1944)
49. HAZUS-MH: Multi-hazard loss estimation methodology - earthquake model (technical manual). Tech. Rep. MH MR5, Federal Emergency Management Agency, Washington (2010)
50. Housner, G.W.: The behavior of inverted pendulum structures during earthquakes. *Bulletin of the Seismological Society of America* **53**(2), 403–417 (1963)
51. Hung, H.H., Liu, K.Y., Ho, T.H., Chang, K.C.: An experimental study on the rocking response of bridge piers with spread footing foundations. *Earthquake Engineering & Structural Dynamics* **40**(7), 749–769 (2011)
52. Jeon, J.S., Shafieezadeh, A., Lee, D.H., Choi, E., DesRoches, R.: Damage assessment of older highway bridges subjected to three-dimensional ground motions: characterization of shear–axial force interaction on seismic fragilities. *Engineering Structures* **87**, 47–57 (2015)
53. Kafali, C., Grigoriu, M.: Rehabilitation decision analysis. In: *Proceedings of the Ninth International Conference on Structural Safety and Reliability*. Rotterdam, Netherlands (2005)
54. Kalliontzis, D., Schultz, A.E.: Characterizing the in-plane rocking response of masonry walls with unbonded posttensioning. *Journal of Structural Engineering* **143**(9), 04017110 (2017)
55. Kawashima, K., MacRae, G.A., Hoshikuma, J.i., Nagaya, K.: Residual displacement response spectrum. *Journal of Structural Engineering* **124**(5), 523–530 (1998)
56. Konstantinidis, D., Makris, N.: Experimental and analytical studies on the response of 1/4-scale models of freestanding laboratory equipment subjected to strong earthquake shaking. *Bulletin of Earthquake Engineering* **8**(6), 1457–1477 (2010)
57. Lee, W.K., Billington, S.L.: Performance-based earthquake engineering assessment of a self-centering, post-tensioned concrete bridge system. *Earthquake Engineering & Structural Dynamics* **40**(8), 887–902 (2011)
58. Mackie, K., Stojadinovic, B.: Residual displacement and post-earthquake capacity of highway bridges. In: *Proceedings of the 13th World Conference on Earthquake Engineering*, pp. 1–16. Vancouver, Canada (2004)
59. Mackie, K., Stojadinović, B.: Post-earthquake functionality of highway overpass bridges. *Earthquake Engineering & Structural Dynamics* **35**(1), 77–93 (2006)
60. Mackie, K.R., Wong, J.M., Stojadinović, B.: Post-earthquake bridge repair cost and repair time estimation methodology. *Earthquake Engineering & Structural Dynamics* **39**(3), 281–301 (2010)
61. Makris, N.: The role of the rotational inertia on the seismic resistance of free-standing rocking columns and articulated frames. *Bulletin of the Seismological Society of America* **104**(5), 2226–2239 (2014)

62. Makris, N., Vassiliou, M.F.: Planar rocking response and stability analysis of an array of free-standing columns capped with a freely supported rigid beam. *Earthquake Engineering & Structural Dynamics* **42**(3), 431–449 (2013)
63. Mander, J.B.: Fragility curve development for assessing the seismic vulnerability of highway bridges. Tech. rep., University at Buffalo (1999)
64. Mantawy, I.M., Thonstad, T., Sanders, D.H., Stanton, J.F., Eberhard, M.O.: Seismic performance of precast, pretensioned, and cast-in-place bridges: Shake table test comparison. *Journal of Bridge Engineering* **21**(10), 04016071 (2016)
65. Marriott, D., Pampanin, S., Bull, D., Palermo, A.: A probabilistic seismic loss assessment of advanced post-tensioned precast bridge systems. In: *Proceedings of the New Zealand Society for Earthquake Engineering Annual Conference*. Wellington, New Zealand (2009)
66. Marriott, D., Pampanin, S., Palermo, A.: Quasi-static and pseudo-dynamic testing of unbonded post-tensioned rocking bridge piers with external replaceable dissipaters. *Earthquake Engineering & Structural Dynamics* **38**(3), 331–354 (2009)
67. Mashal, M., Palermo, A.: Low-damage seismic design for accelerated bridge construction. *Journal of Bridge Engineering* **24**(7), 04019066 (2019)
68. Meek, J.W.: Effects of foundation tipping on dynamic response. *Journal of the Structural Division* **101**(7), 1297–1311 (1975)
69. Moehle, J., Deierlein, G.G.: A framework methodology for performance-based earthquake engineering. In: *Proceedings of the 13th World Conference on Earthquake Engineering*, Paper No 679. Vancouver, B.C., Canada (2004)
70. Muntasir Billah, A., Alam, M.S.: Seismic fragility assessment of concrete bridge pier reinforced with superelastic shape memory alloy. *Earthquake Spectra* **31**(3), 1515–1541 (2015)
71. Neter, J., Kutner, M.H., Nachtsheim, C.J., Wasserman, W.: *Applied linear statistical models*, vol. 4. McGraw-Hill (1996)
72. Oliveto, G., Calio, I., Greco, A.: Large displacement behaviour of a structural model with foundation uplift under impulsive and earthquake excitations. *Earthquake Engineering & Structural Dynamics* **32**(3), 369–393 (2003)
73. Padgett, J.E., DesRoches, R.: Bridge functionality relationships for improved seismic risk assessment of transportation networks. *Earthquake Spectra* **23**(1), 115–130 (2007)
74. Palermo, A., Pampanin, S.: Enhanced seismic performance of hybrid bridge systems: Comparison with traditional monolithic solutions. *Journal of Earthquake Engineering* **12**(8), 1267–1295 (2008)
75. Panagiotou, M., Trono, W., Jen, G., Kumar, P., Ostertag, C.P.: Experimental seismic response of hybrid fiber-reinforced concrete bridge columns with novel longitudinal reinforcement detailing. *Journal of Bridge Engineering* **20**(7), 04014090 (2014)
76. Pecker, A.: Enhanced seismic design of shallow foundations: example of the Rion Antirion bridge. In: *4th Athenian lecture on Geotechnical Engineering*, Hellenic Society of Soil Mechanics and Geotechnical Engineering, Athens, Greece, (2006)
77. Pelekis, I., Madabhushi, G.S., DeJong, M.J.: Seismic performance of buildings with structural and foundation rocking in centrifuge testing. *Earthquake Engineering & Structural Dynamics* **47**(12), 2390–2409 (2018)
78. Prieto, F., Lourenço, P.B., Oliveira, C.: Impulsive dirac-delta forces in the rocking motion. *Earthquake Engineering & Structural Dynamics* **33**(7), 839–857 (2004)
79. Psycharis, I.N.: Effect of base uplift on dynamic response of s dof structures. *Journal of Structural Engineering* **117**(3), 733–754 (1991)
80. Psycharis, I.N., Fragiadakis, M., Stefanou, I.: Seismic reliability assessment of classical columns subjected to near-fault ground motions. *Earthquake Engineering & Structural Dynamics* **42**(14), 2061–2079 (2013)
81. Reggiani Manzo, N., Vassiliou, M.F.: Displacement-based analysis and design of rocking structures. *Earthquake Engineering & Structural Dynamics* **48**(14), 1613–1629 (2019)
82. Saad, A.S., Sanders, D.H., Buckle, I.G.: Experimental evaluation of bridge column foundation rocking behavior. *Journal of Bridge Engineering* **23**(11), 04018088 (2018)
83. Shinozuka, M., Feng, M.Q., Lee, J., Naganuma, T.: Statistical analysis of fragility curves. *Journal of Engineering Mechanics* **126**(12), 1224–1231 (2000)
84. Stein, S.M., Young, G.K., Trent, R.E., Pearson, D.R.: Prioritizing scour vulnerable bridges using risk. *Journal of Infrastructure Systems* **5**(3), 95–101 (1999)
85. Thonstad, T., Kennedy, B., Schaefer, J., Eberhard, M., Stanton, J.: Cyclic tests of precast pretensioned rocking bridge-column subassemblies. *Journal of Structural Engineering* **143**(9), 04017094 (2017)
86. Thonstad, T., Mantawy, I.M., Stanton, J.F., Eberhard, M.O., Sanders, D.H.: Shaking table performance of a new bridge system with pretensioned rocking columns. *Journal of Bridge Engineering* **21**(4), 04015079 (2016)

87. Trono, W., Jen, G., Panagiotou, M., Schoettler, M., Ostertag, C.P.: Seismic response of a damage-resistant recentering posttensioned-hyfrc bridge column. *Journal of Bridge Engineering* **20**(7), 04014096 (2014)
88. Truniger, R., Vassiliou, M.F., Stojadinovic, B.: An analytical model of a deformable cantilever structure rocking on a rigid surface: experimental validation. *Earthquake Engineering & Structural Dynamics* **44**(15), 2795–2815 (2015)
89. USGS: Earthquake probabilities in the San Francisco Bay region: 2002–2031. Tech. Rep. 03-214, Working Group on California Earthquake Probabilities, United States Geological Survey (2003)
90. Vamvatsikos, D., Cornell, C.A.: Incremental dynamic analysis. *Earthquake Engineering & Structural Dynamics* **31**(3), 491–514 (2002)
91. Vassiliou, M.F.: Seismic response of a wobbling 3D frame. *Earthquake Engineering & Structural Dynamics* **47**(5), 1212–1228 (2017)
92. Vassiliou, M.F., Burger, S., Egger, M., Bachmann, J.A., Broccardo, M., Stojadinovic, B.: The three-dimensional behavior of inverted pendulum cylindrical structures during earthquakes. *Earthquake Engineering & Structural Dynamics* **46**(14), 2261–2280 (2017)
93. Vassiliou, M.F., Mackie, K.R., Stojadinovic, B.: Dynamic response analysis of solitary flexible rocking bodies: modeling and behavior under pulse-like ground excitation. *Earthquake Engineering & Structural Dynamics* **43**(10), 1463–1481 (2014)
94. Vassiliou, M.F., Mackie, K.R., Stojadinovic, B.: A finite element model for seismic response analysis of deformable rocking frames. *Earthquake Engineering & Structural Dynamics* **46**(3), 447–466 (2017)
95. Vassiliou, M.F., Truniger, R., Stojadinovic, B.: An analytical model of a deformable cantilever structure rocking on a rigid surface: development and verification. *Earthquake Engineering & Structural Dynamics* **44**(15), 2775–2794 (2015)
96. Wen, Y.K., Kang, Y.: Minimum building life-cycle cost design criteria. I: Methodology. *Journal of Structural Engineering* **127**(3), 330–337 (2001)
97. Wen, Y.K., Kang, Y.: Minimum building life-cycle cost design criteria. II: Applications. *Journal of Structural Engineering* **127**(3), 338–346 (2001)
98. White, S., Palermo, A.: Quasi-static testing of posttensioned nonemulative column-footing connections for bridge piers. *Journal of Bridge Engineering* **21**(6), 04016025 (2016)
99. Xie, Y., Zhang, J., DesRoches, R., Padgett, J.E.: Seismic fragilities of single-column highway bridges with rocking column-footing. *Earthquake Engineering & Structural Dynamics* **48**(7), 843–864 (2019)
100. Zhang, J., Xie, Y., Wu, G.: Seismic responses of bridges with rocking column-foundation: A dimensionless regression analysis. *Earthquake Engineering & Structural Dynamics* **48**(1), 152–170 (2019)
101. Zheng, Y., Dong, Y., Li, Y.: Resilience and life-cycle performance of smart bridges with shape memory alloy (SMA)-cable-based bearings. *Construction and Building Materials* **158**, 389–400 (2018)